Electro-Mechanical Design and Testing of a Prototype Low-Cost Rheometer

by

Makita F. Erni

Submitted to the Department of Mechanical Engineering
in Partial Fulfillment of the Requirements for the Degree of

Bachelor of Science in Mechanical Engineering

at the

Massachusetts Institute of Technology

June 2022

Signature of Author: ……..
Department of Mechanical Engineering
May 6, 2022

Certified by: ……...
David L. Trumper
Professor of Mechanical Engineering
Thesis Supervisor

Certified by: ……...
Kenneth Kamrin
Associate Professor of Mechanical Engineering
Undergraduate Officer

Electro-Mechanical Design and Testing of a Prototype Low-Cost Rheometer

by

Makita F. Erni

Submitted to the Department of Mechanical Engineering
on May 6, 2022 in Partial Fulfillment of the
Requirements for the Degree of

Bachelor of Science in Mechanical Engineering

ABSTRACT

Rheology is a key part of modern society, but the devices used to measure complex fluids are large and expensive, making them unobtainable for individuals or small organizations. This thesis presents the first and second prototypes of an effort to design an accurate but low-cost (<$200) rheometer using fused deposition modeling 3-dimensional printing (FDM 3D printing) and off-the-shelf components. Both designs utilized a cylinder rotating concentrically inside a cylindrical cup of sample fluid. The first prototype used an encoded direct current (DC) motor to rotate at a constant rate while measuring the motor current draw to estimate torque and was able to measure a fluid viscosity standard with $\eta = 100$ Pa.s within 17% of the known value. The second prototype used a microstepping stepper motor to rotate at a constant rate while using a loadcell to measure the reaction torque on the cup used to hold the sample and was able to measure a $\eta = 0.1$ Pa.s sample within 18% of the actual value. The second prototype was also able to measure viscosity vs shear rate curves for shear-thinning fluids over shear rates from 22.6 to 3.8 s^{-1} all at a cost less than 0.4% that of a laboratory rheometer (DHR-3; TA Instruments) which was used to obtain the comparison data. Finally, this thesis suggests changes to improve the accuracy and versatility of future designs.

Thesis Supervisor: David L. Trumper

Title: Professor of Mechanical Engineering

Acknowledgments

I would like to give special thanks to Crystal Owens for the project idea and helping me through every phase of the project. To Professor Trumper for advising me through this project, encouraging me to take on this thesis project, and helping me find the best direction for the design. To Professor McKinley and his lab for supporting this project and advising me. Finally, to Dan at LMP, my floormates on $\pi\tau$z, and my parents for the essential help brainstorming and troubleshooting, and the access to 3D printers and other tools needed to complete this project.

Table of Contents

List of Figures

List of Tables

1. Introduction

This thesis describes the design, construction, and testing of a prototype low-cost rheometer which was inspired by prior work of Owens, et al. with 3D printing vanes that can be used with existing rheometers [1]. The final goal of this project is to create an open-source rotary rheometer costing less than $200 which can rotate at speeds ranging from 0.01 to 100 RPM and measure fluids with viscosities varying from 0.01 to 10 Pa.s. The goal of the work in this thesis is to take the first step by developing a low-cost design that will meet the desired specifications after further development. The ultimate aspiration of this rheometer is to be deployed as a kit alongside Owens' 3D printed vanes.

This project is important because viscosity, which is a fluid's resistance to shear, and the other rheological properties of fluids are essential to everyday life. Reducing the cost threshold to learn about and measure them will expose a new world to schools, hobbyists, and professionals as well as give labs the option of a customizable and 3D printable rheometer they can modify for their specialized applications. Examples of where viscosity and other rheological properties are important include concrete, painting, injection molding, food, and something that invaded the world's lives in 2020: hand sanitizer.

Hand sanitizer is carefully engineered to be shear-thinning, meaning its viscosity decreases as the shear rate increases [2]. The practical application for this is that it can have a high viscosity while in storage, but it can still be dispensed like a lower viscosity liquid when it is pumped the shear rate increases lowering the viscosity [2]. A low-cost rheometer would allow students to measure and understand this and would allow hobbyists to tune properties like this in their homemade hand sanitizers, foods, and other fluids.

Viscosity is also key to the process used to make this rheometer: 3D printing. If the viscosity of the filament is too high, the 3D printer's nozzle can clog, and if the viscosity is too low then material can leak out of the nozzle at a rate different than that desired [3]. Ideally, a 3D printed material would be shear thinning so it stays in place after being deposited [3]. The material used to make this rheometer, PLA, is shear thinning [4]. While this version of the rheometer cannot withstand the temperatures required to melt PLA, the advantage of a simple open-source low-cost modifiable rheometer is that a version can be made for the more specialized application of verifying filament viscosities and finding the best printing temperature for each filament.

2. Background

2.1 Rotary Rheometer

Rotary rheometers work by rotating an axially symmetric object of known geometry which is in contact with the liquid under test, shearing the fluid between the rotating geometry and a static surface. The shear rates and shear stresses can be calculated from the rotation rate, torque, and known geometry [1]. Viscosity (η) in pascal-seconds is a function of shear stress (σ) in pascals and shear rate ($\dot{\gamma}$) in inverse seconds as shown in Equation 1 [5].

$$\eta = \frac{\sigma}{\dot{\gamma}} \tag{1}$$

There are many types of geometries that can be used including parallel plates and vanes. Both version 1 and version 2 were tested using a rotating cylindrical geometry in a stationary cylindrical cup. Shear rate and shear stress were calculated for this geometry with Equations 2 and 3 respectively [1]. In Equations 2 and 3, Ω is the rotation rate in radians per second, τ is the torque

required to rotate the cylinder at Ω in newton-meters, and $R_{Cylinder}$, R_{Cup}, and $L_{Cylinder}$ represent the radius of the cylinder and cup, and the length of the cylinder respectively in meters.

$$\dot{\gamma} = \frac{2\Omega}{1-\left(\frac{R_{Cylinder}}{R_{Cup}}\right)^2} \tag{2}$$

$$\sigma = \frac{\tau}{2\pi \cdot \left(R_{Cylinder}\right)^2 \cdot L_{Cylinder} \cdot \left(1+\frac{2 \cdot R_{Cylinder}}{3 \cdot L_{Cylinder}}\right)} \tag{3}$$

Another important fluid property that can be measured is the Reynolds number. The Reynolds number compares the ratio of inertial and viscous forces [6]. It is used to determine if a fluid is in laminar or turbulent flow [7]. The Reynolds number is found using Equation 4 where *Re* is the Reynolds number, ρ is the fluid density in kilograms per cubic meter, *v* is the velocity of the fluid in meters per second, *L* is the gap between the rotating geometry and the cup in meters, and μ is the fluid viscosity in pascal-seconds [6].

$$Re = \frac{\rho v L}{\mu} \tag{4}$$

2.2 Measuring Torque

Measuring torque is one of the most challenging parts of rotary rheometer design [8]. With the low torques involved in measuring viscosity, the noise of the system or the environment can confound the torque measurement. One direct way to measure torque would be to measure the inline torque on the drive shaft, but commercial inline torque transducers can be expensive and making one can be complicated with the quality of data from the strain gauges being heavily dependent on the quality of the installation [9]. For this project, two alternatives were explored: estimating torque from motor current draw, and measuring the reaction torque on the cup. In DC motors, the torque (*T*) in Nm is related to the current (*I*) in A with a linear relationship as shown in Equation 5 where *k* is the motor constant in Nm/A and I_0 is the current lost to factors such as kinetic friction in A [10]. This method was used for the version 1 design in Section 3.

$$T = k \cdot (I - I_0) \tag{5}$$

The second method used to measure torque was to measure the reaction torque on the cup. To accomplish this, the cup needed to be able to make small rotations. This was accomplished using a flexure which acts like a zero-friction bearing for small rotations [11]. A wheatstone-bridge configuration beam loadcell was used to measure the torque. Loadcells are typically made of a machined geometry with bonded strain gauges [5]. The strain gauges change resistance based on their deformation, meaning they can be used to electronically measure the deformation of the part they are bonded to, which is related to the force applied to that part [5]. This method was used for the version 2 design in Section 4.

2.3 Stepper Motor Micro Stepping

Stepper motors rotate by moving or stepping between discrete locations in a circular pattern [12]. Typical stepper motors have 200 steps per rotation, but many stepper controllers allow each step to be divided into multiple micro steps with some being able to divide each step into 256

micro steps resulting in 51,200 steps per rotation [12]. Micro stepping allows a stepper motor to rotate smoothly which is especially useful at slow speeds [12]. Stepper motors typically have 2 phases, and the controller sends an approximation of a current sine wave into one phase and a cosine wave into the other phase [13]. The version 2 design in Section 4 utilizes a stepper motor.

3. Version 1 Rheometer

The initial iteration of this project, referred to as version 1, estimated torque by relating it to the current driving a motor. Due to the COVID-19 Pandemic, it was completed almost entirely remotely and without access to advanced measurement tools such as a Prony brake. Version 1 is shown in Figure 1 and Figure 2. This design uses a 3D printed cup with the testing apparatus attaching directly to the cup. This setup cost less than $150, details in Subsection 6.1 Appendix A.

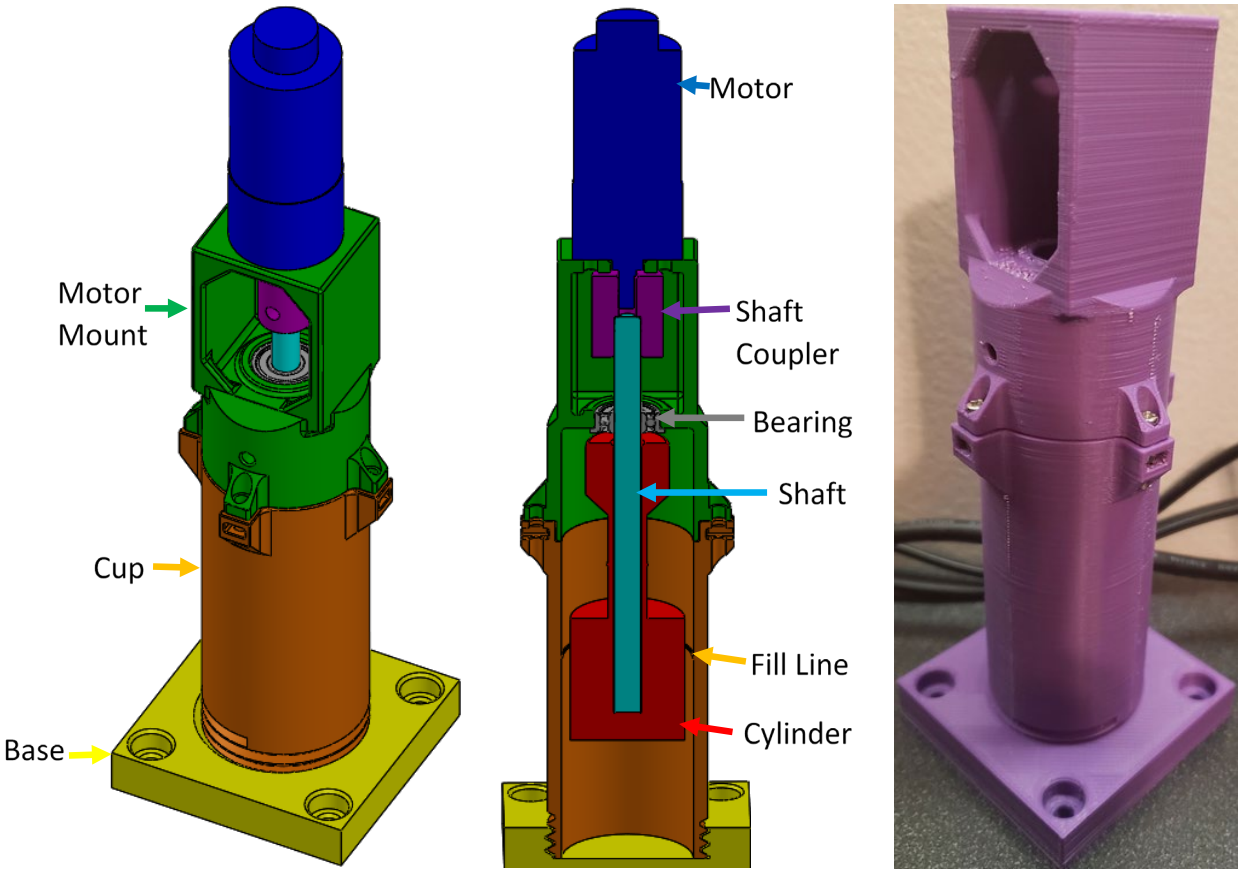

Figure 1: CAD of the completed version 1 test assembly and a 3D printed prototype. In the CAD, the motor mount is green, the cylinder is red, the base is yellow, the cup is orange, the bearing is grey, the shaft coupler is purple, the shaft is aqua, and the motor is blue. The assembly is approximately 8.2” tall with the motor and 5.9” tall without the motor. The base is a 2.2” square.

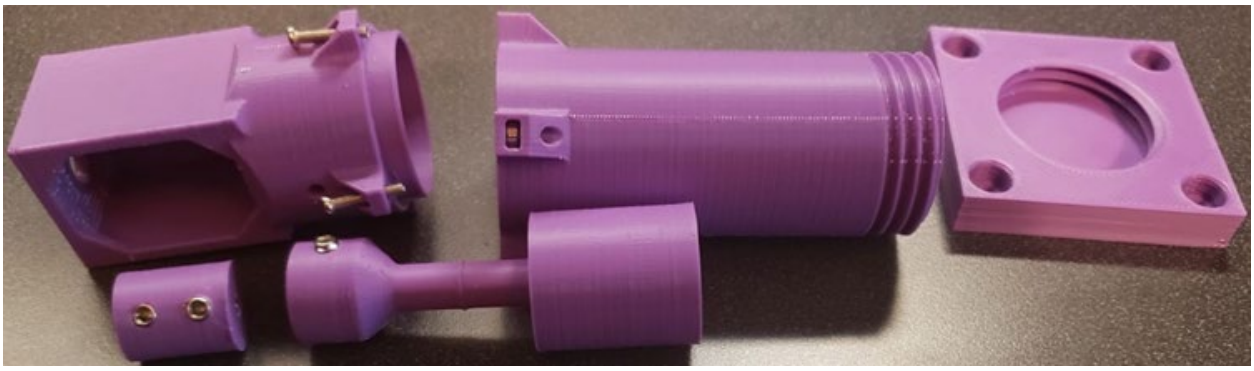

Figure 2: A disassembled 3D printed prototype of version 1.

3.1 Version 1 Rheometer Design

3.1.1 Cylinder Testing Geometry

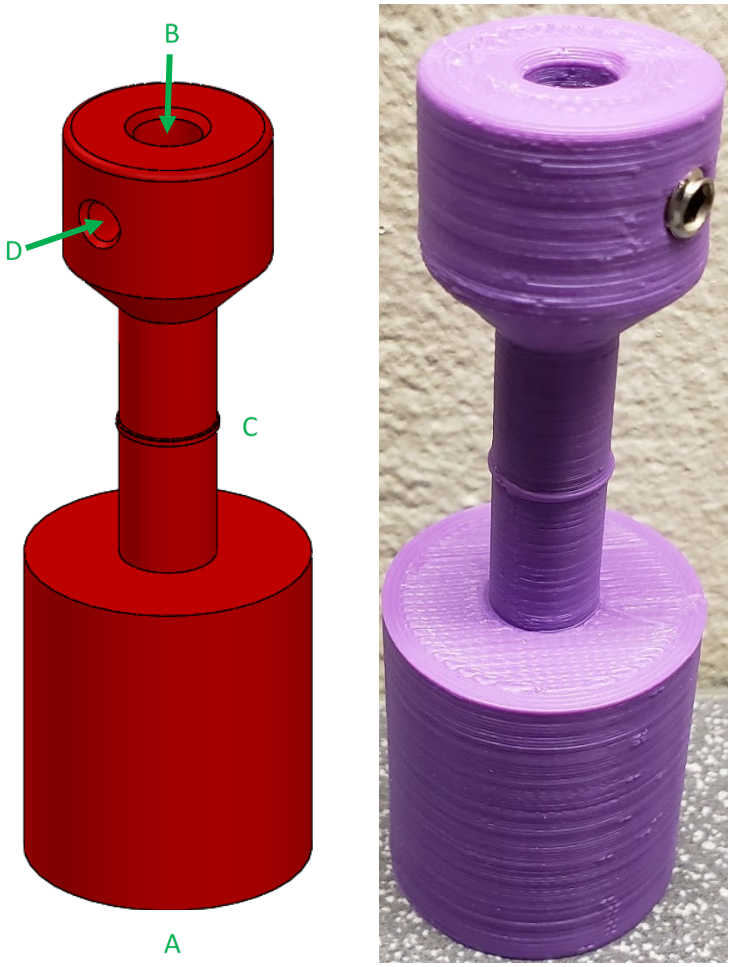

Figure 3: CAD of the version 1 cylinder end effector and a 3D printed prototype. This part is approximately 2.9” tall with a diameter of about 1”.

As shown in Figure 3, the cylinder was printed with the bottom surface (A) flat on the print bed, 4 shells to help prevent leaking by increasing the number of layers before the infill starts, and no supports. To give this part extra rigidity, the shaft goes into the hole in the top (B) and 2.6" deep into this part. The small extrusion (C) part way up the small cylinder is a fill line to help the user during sample testing. A 4-arm vane design was considered, but the cylindrical design was chosen for initial testing for its simplicity and versatility.

The 2 horizontal holes (D) are screw holes. While it is typically not recommended to tap directly into 3D printed plastic, previous personal experiences have shown that coarse threads can be successfully and repeatedly used for light duty applications. 10-24 set screws had coarse enough threads to be repeatedly used in 3D printed plastic as demonstrated by the threads never being the first feature to fail. Instead, cracking initiated along the layer lines, but this only occurred after tests with continuous high torque that should never be encountered in normal use. Based on trial and error, the holes should be reamed to the correct tap size, and a tapered tap should be used. If a screw or a non-tapered tap is used to cut the threads, there is a risk of cracking the part along the layer lines.

3.1.2 Motor Mount

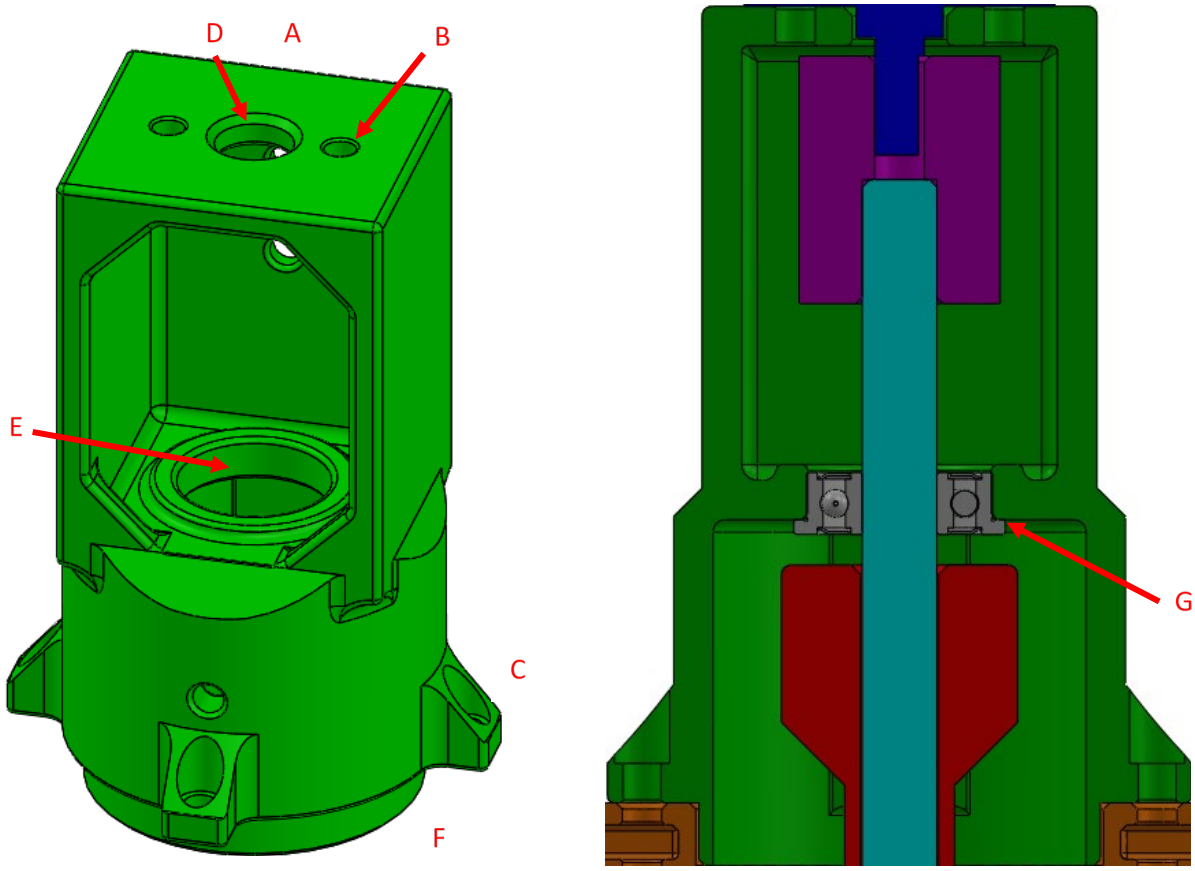

Figure 4: CAD of the version 1 motor mount. This part is approximately 2.8" tall.

As shown in Figure 4 and Figure 5, the motor mount was printed with the top surface (A) flat on the print bed so support material would not prevent the bearing flange from having a flat surface to press against (G), 1 shell, and supports inside the part and outside for the screw mounts. The additional horizontal holes are for tool access and the vertical holes (B (x2) and C (x4)) are for

screws, the motor (D), and the bearing (E). The large cutout in the middle is to install the shaft coupler. The smaller circular extrusion (F) at the bottom of the motor mount is designed to go into a mating circular cutout in the cup to align the two parts and prevent leaks. The chamfers on the screw mounts (C) were added to make the part easier to print. The bearing is designed to press fit into the bearing hole (E) with the flange on the bottom.

Figure 5: Version 1 motor mount 3D printed prototype.

3.1.3 Cup

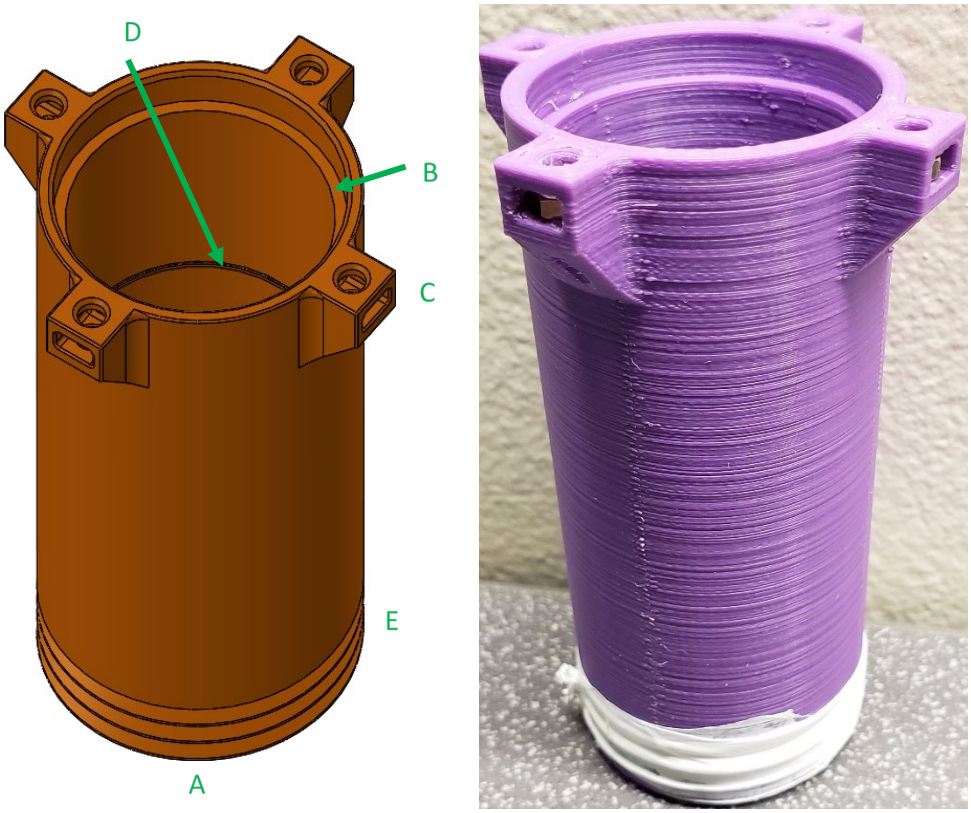

Figure 6: CAD of the version 1 cup and a 3D printed prototype. This part is approximately 3.3” tall.

As shown in Figure 6, the cup was printed with the bottom surface (A) flat on the print bed so the ledge (B) that interacts with the motor mount would be free of support material and relatively flat, 4 shells to prevent leaking, and supports outside for the 4 screw mounts (C). The circular cutout (B) near the top of the cup is designed to support the mating circular extrusion on the motor mount to align the two parts and prevent leaks. The square cutouts (C) in the screw mounts are for nuts. The extrusion (D) in the cup is a fill line.

The threads (E) on the bottom screw into the base. Attaching the cup using screws was considered, but threading the cup onto the base was chosen because it made the system easier to clean. This did initially result in some issues with leaking, but that was resolved by adding 5 to 7 layers of Teflon tape around the threads on the cup. After adding the Teflon tape, no leaks were observed while letting it sit with water to the fill line for two hours. There was also no noticeable change in water levels during leak testing which if present could have indicated that some of the water seeped into the part.

3.1.4 Base

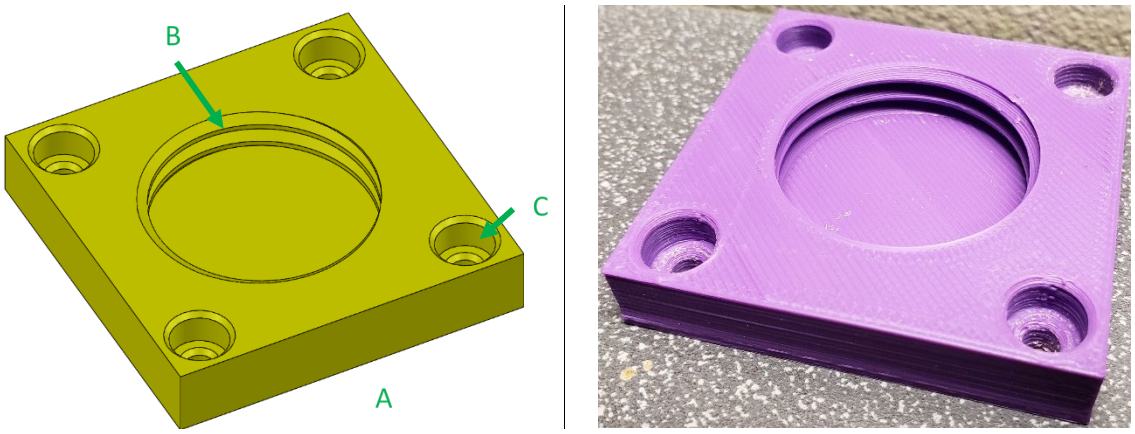

Figure 7: CAD of the version 1 base and a 3D printed prototype. This part is approximately 0.4” tall and is an approximately 2.2” square.

As shown in Figure 7, the base was printed with the large square bottom surface (A) flat on the print bed, 4 shells to help prevent leaking, and no supports. The threads (B) allow the cup to easily be attached to the base. The 4 holes in the corners (C) allow it to be screwed onto a larger base such as a block of wood for stability.

3.1.5 Shaft Coupler

Initially, a commercially available rigid shaft coupler was chosen because it was thought a flexible shaft coupler could influence instantaneous torque readings. This purchased rigid shaft coupler was found to contribute a visible amount of runout due to oversized shaft holes, so it was replaced with a 3D printed version which is shown in Figure 8 and had less visible runout. To further reduce runout from this part, the best method found was to print a shaft coupler with set screw holes and one through hole smaller than 4mm, drill it out to 4mm for the motor shaft, and then drill half of it out to 6mm for the drive shaft. The holes for the set screws were tapped using a tapered tap as described in Subsection 3.1.1. A reinforced version shown in Figure 9 was made

after experiencing issues with the shaft coupler breaking during stall tests. The reinforced coupler was also coated in a thin coat of super glue to reduce risk of delamination.

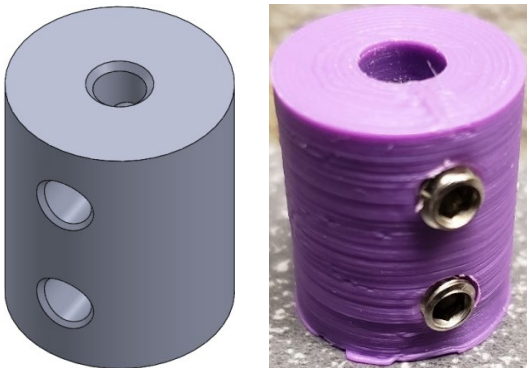

Figure 8: Standard version 1 drilled out shaft coupler. This part was printed with the flat surface on the print bed, 2 shells for the threads, and no supports. This part is approximately 0.8” tall and 0.6” in diameter.

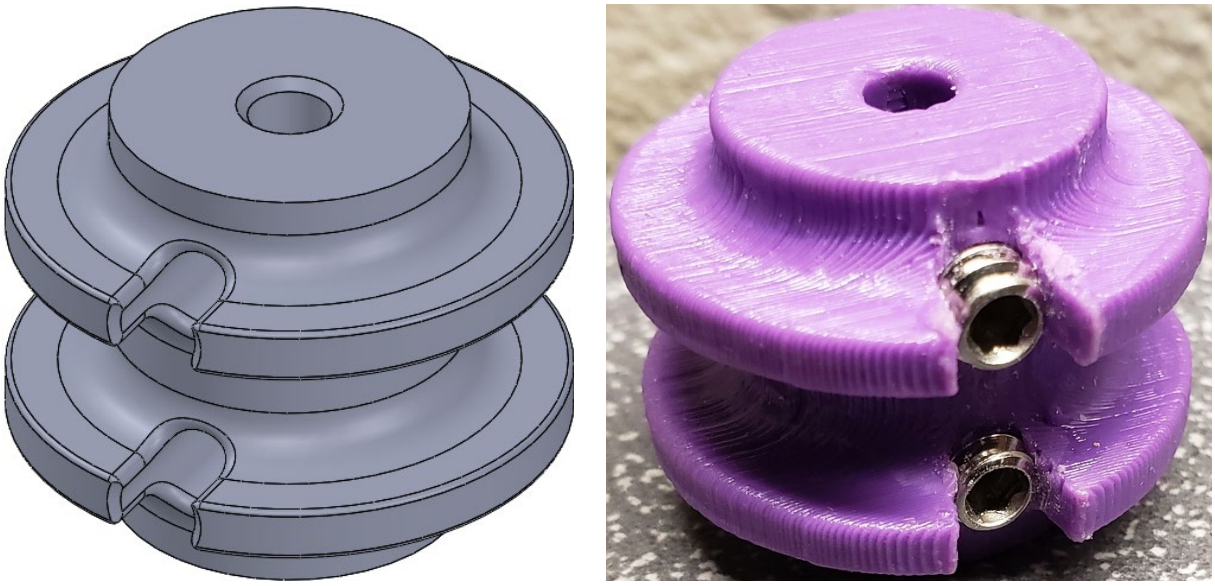

Figure 9: The version 1 reinforced shaft coupler was printed sideways so the layer lines were perpendicular to where cracking was occurring, 2 shells for the threads, and supports for the cylinder. This part is approximately 0.8” tall and 1” in diameter.

3.1.6 Version 1 Electronics Wiring Diagram

Figure 10 shows the wiring diagram for version 1. The main components are 2 Arduino Unos, a current sensor, a motor controller, and a motor with a built-in encoder. The first Arduino collects rotation rate data and controls the motor controller which controls the motor. The second Arduino collects data from the current sensor which measures the current into the motor. 2 Arduinos were used to simplify coding for this prototype.

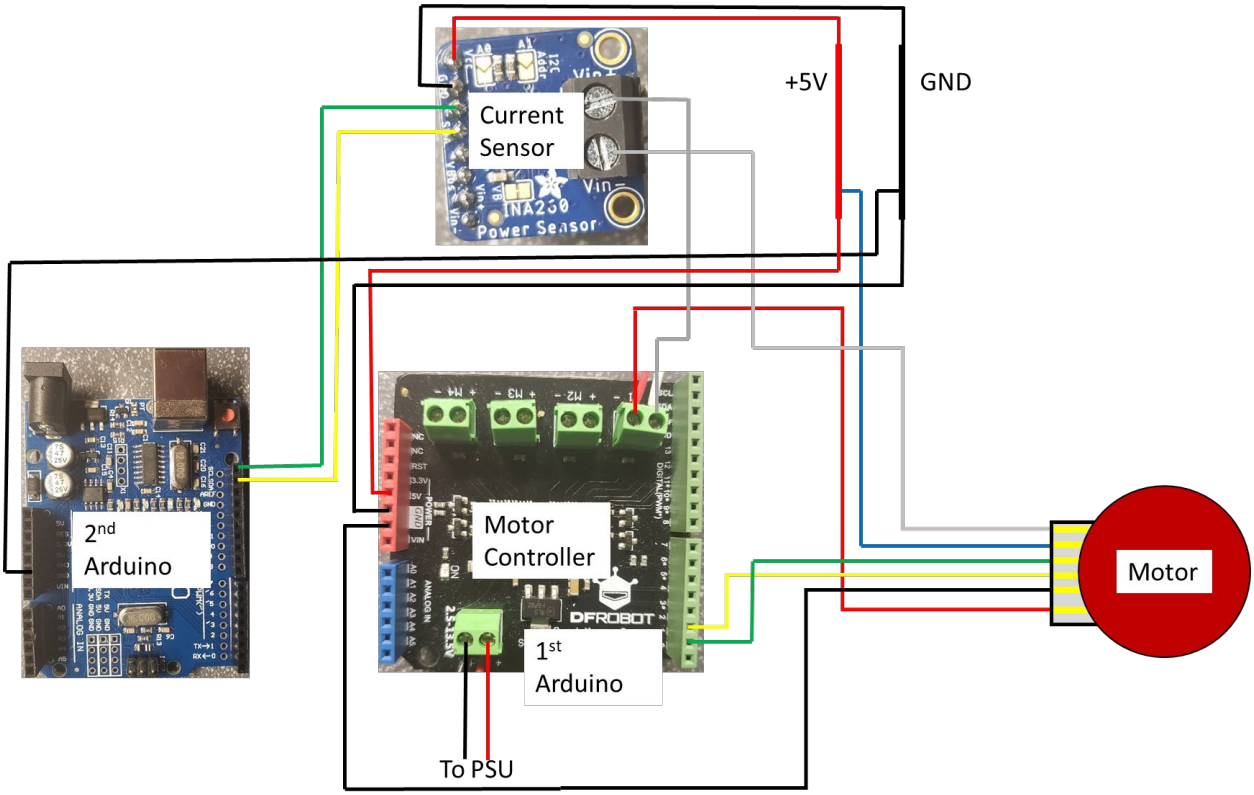

Figure 10: Wiring diagram for version 1. It includes 2 Arduino Unos, a current sensor, a motor controller, and a motor. The 1st Arduino is not pictured because it is underneath the motor controller shield which passes the connections through the headers to the 1st Arduino.

3.2 Version 1 DC Motor Testing

This design requires a known relationship between motor current and torque to measure viscosity. As this was done without access to a lab, a simple Prony brake detailed in Subsection 3.2.1 was made to estimate the torque-current relationship previously shown in Equation 5.

Inputs:

- Variable voltage through pulse-width modulation (PWM) with 255 increments from 0V to the maximum power supply voltage of 6V
- Normal force on the shaft with the Prony brake.

Outputs:

- Current and voltage through current sensing chip
  - Samples every 140 microseconds
  - Averages 256 readings
  - Accuracy of 1.5 mA
  - Current range of 15A
  - Voltage range of 36V
- Torque from the Prony brake's lever arm and a kitchen scale indicating weight change
- Speed from motor encoder

3.2.1 Prony Brake

The Prony brake design shown in Figure 11 was inspired by a Hackaday project and works by applying a variable frictional force and torque to the output shaft [14]. The washers on the end of the bolt add weight to reduce movement and bouncing of the head when force is applied. The applied torque is found by multiplying the average force on the scale by the lever arm of the Prony brake. Potential causes of error when this was used for this project was the use of a D shaft which caused a varied torque to be applied to the shaft as it rotated, the runout which caused the tip to move around the scale, and the sample rate of the scale. There were also difficulties adjusting the Prony brake to test the mid-torque range. The resulting Torque-Current approximation is shown in Figure 12.

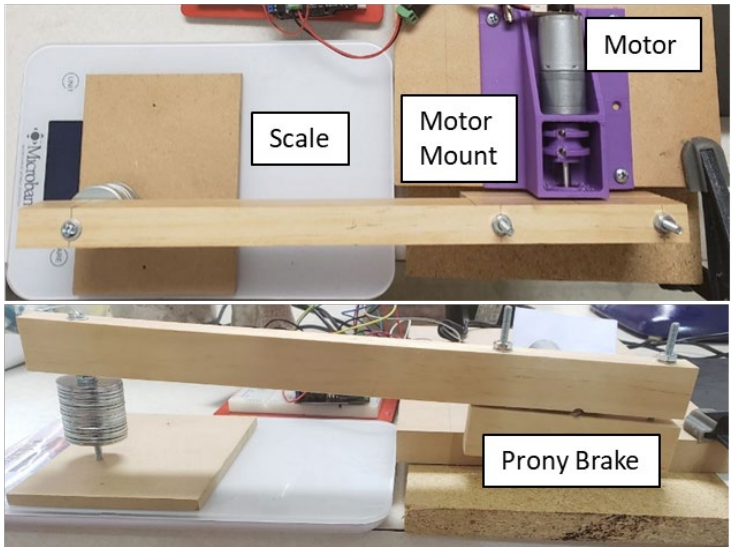

Figure 11: The Prony brake mounted onto the testing assembly.

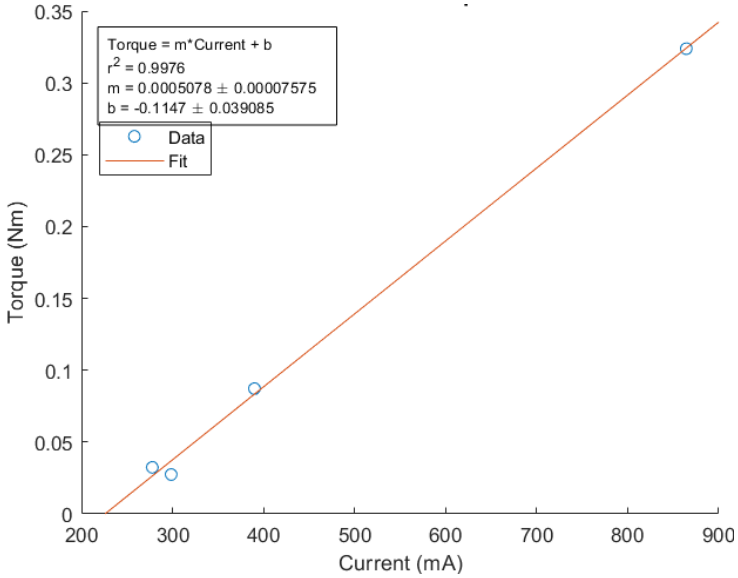

Figure 12: This figure was generated using the version 1 setup and the Prony break described above. It shows how average current and torque are related and gives a fit equation that was used for viscosity calculations in Subsection 3.3. The data was found using the scale and the current sensor.

3.3 Version 1 Viscosity Testing: Methods, Results, and Discussion

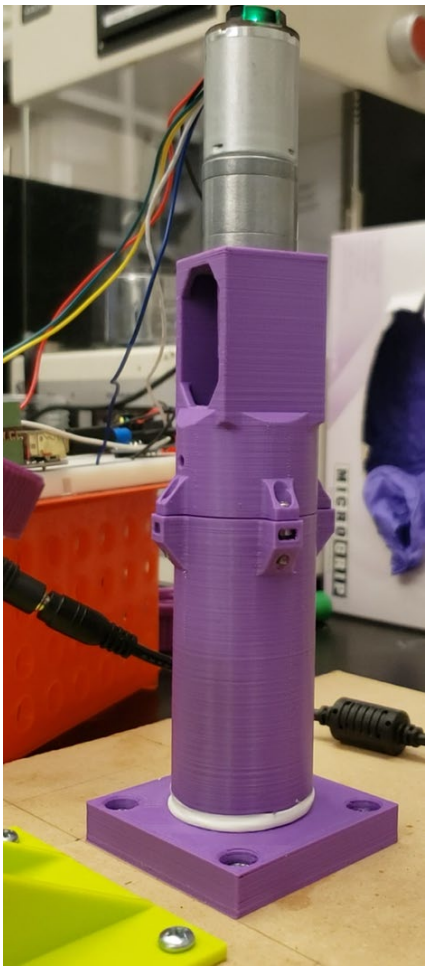

Figure 13: This is the setup used for testing fluids with version 1.

To take a measurement with version 1, the base is secured to a larger base such as a block of wood and the cup is screwed onto the base as shown in Figure 13. The substance under test is then added until it is up to the fill line on the cup; it is better to slightly overfill it than to under fill it to avoid boundary effects. Next, the motor assembly with a cylinder attached by a shaft and supported by a bearing is screwed onto the cup. A microcontroller-controlled motor controller uses PWM control and feedback from the motor's built-in encoder to sweep multiple angular rotation rates with the motor and find a steady state current reading for each using a current sensor. The current data can be converted into torque estimates using a current-torque relationship found using the Prony brake in Subsection 3.2.1 and shown in Equation 6 where torque is in Nm and Current is in A. The angular rotation rate data and the torque estimate can be used to calculate a viscosity value for the sample using Equations 1, 2, and 3. Samples with viscosities of 1, 10, and 100 Pa.s were tested along with a hair gel. Figure 14 shows the Rotation Rate over time.

$$Torque = 0.0005078 \cdot Current - 0.1147 \quad (6)$$

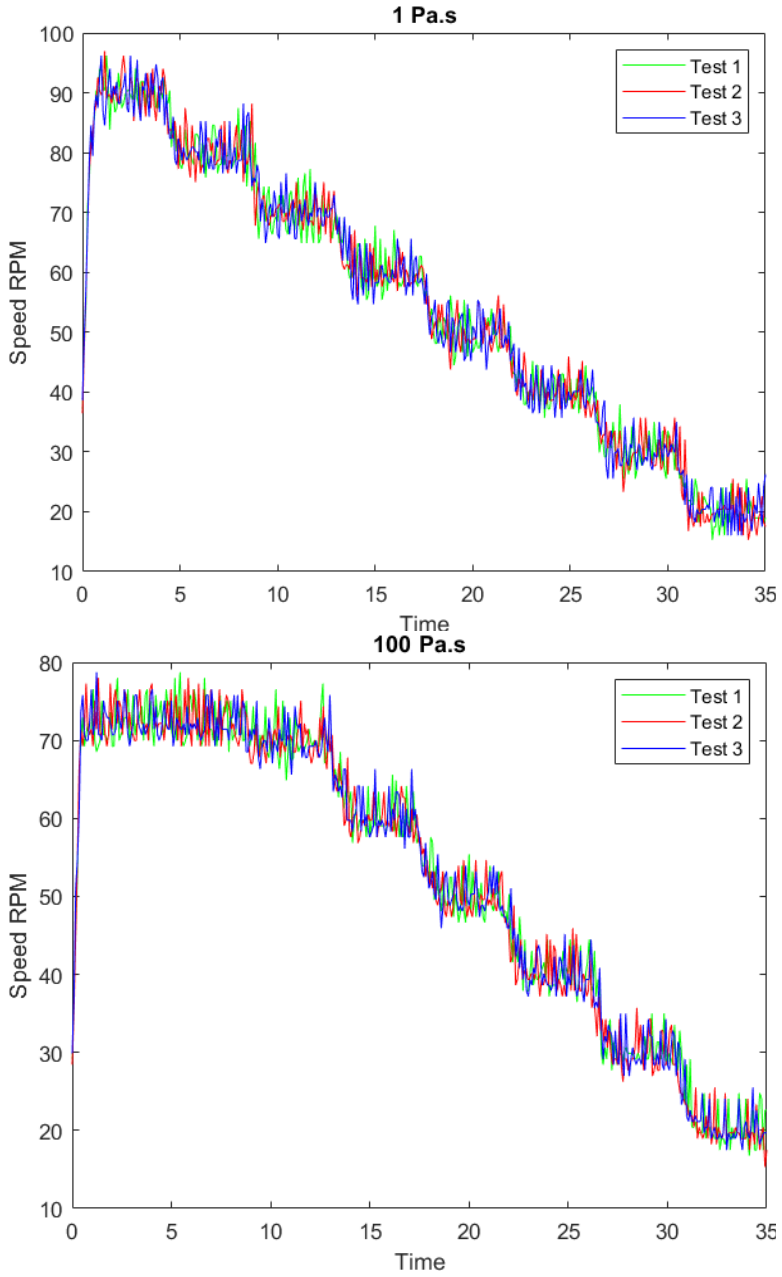

Figure 14: This figure shows the rotation rate data over time for a 1 and 100 Pa.s sample using the version 1 design.

All 4 samples had step functions with noise similar to that shown in Figure 14. The 100 Pa.s sample stayed around 70 RPM for longer than the other samples because that was the maximum speed that could be achieved in that sample. Figure 15 shows the current data over time.

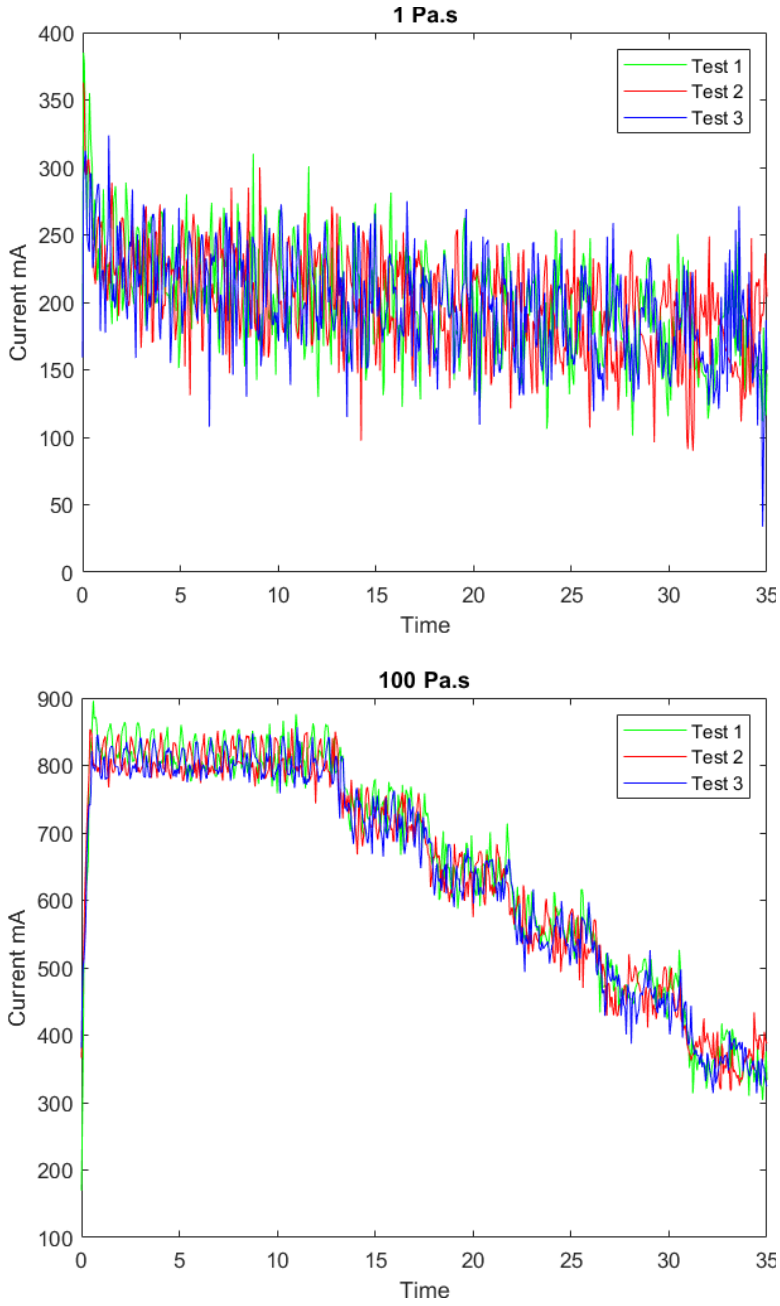

Figure 15: This figure shows the current data over time for a 1 and 100 Pa.s sample using the version 1 design.

For the current data shown in Figure 15, the only sample with a distinct step function was the 100 Pa.s sample. For the other samples the noise in the current measurement was larger than the steps. Details on the noise are in Section 3.4. Figure 16 shows the estimated viscosities.

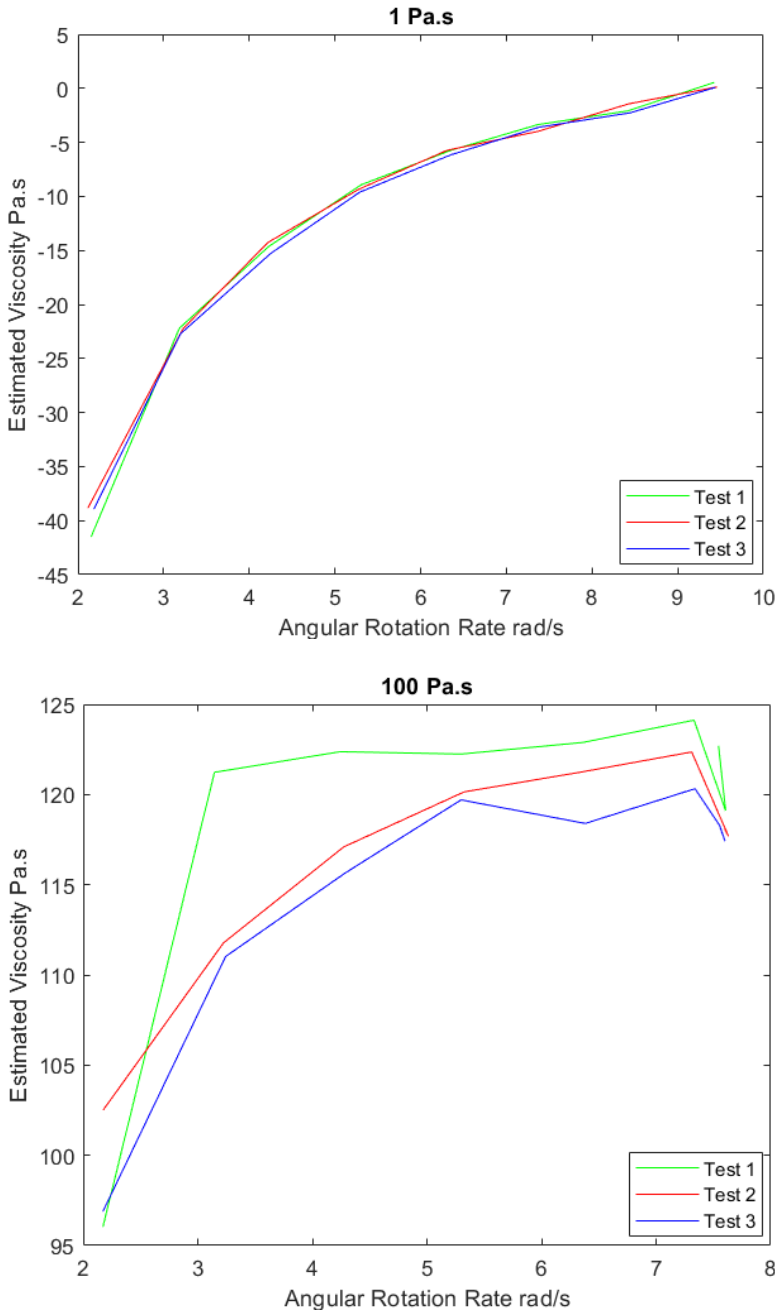

Figure 16: This figure shows the estimated viscosity for a 1 and 100 Pa.s sample using the version 1 design.

Every sample except the 100 Pa.s sample had some negative estimated viscosities because the model in Equation 6 used to convert current to torque assumes that the system would stall at around 226mA and some of the current values found during testing were below that threshold. This indicates the model used to convert current to torque is not accurate for this setup.

The average estimated viscosity for the 100 Pa.s sample is approximately 117 Pa.s which is within 17% of the actual value. The variations in the estimated viscosity for different angular rotation rates could be caused by the noise in the system as described in Section 3.4.

3.4 Version 1 Potential Sources of Error

The 2 primary sources of error are the model in Equation 6 being incorrect, and noise in the system. The error in the model could be due to different environmental conditions as motor testing was done in Utah and sample testing was done in Massachusetts or differences in friction caused by misalignment of the 3D printed parts for testing the motor and for testing a sample. Even though both motor mounts were designed with the same drive train mounting features, variations while 3D printing could have caused differences in alignment of the Prony break motor mount and the sample testing motor mount which could have caused variation in friction. The noise in the system is due to variable friction which creates variation in the measured speeds and currents. This is caused by eccentricities in the system including from the motor, gearbox, and shaft coupler; the rudimentary PWM based control scheme; and the motor transient response.

4. Version 2 Rheometer

Due to the inaccuracy of measuring the torque through the motor current in version 1, the second iteration of this project, version 2, directly measures the reaction torque on the cup using a loadcell. The cup is mounted on a simple cruciform flexure with 1 degree of freedom: rotation about the z-axis. The design as shown in Figure 17 consists of 3 major 3D printed components: the base including the flexure and cup, the motor mount, and the cylinder. This setup cost less than $200, details in Subsection 6.2 Appendix B.

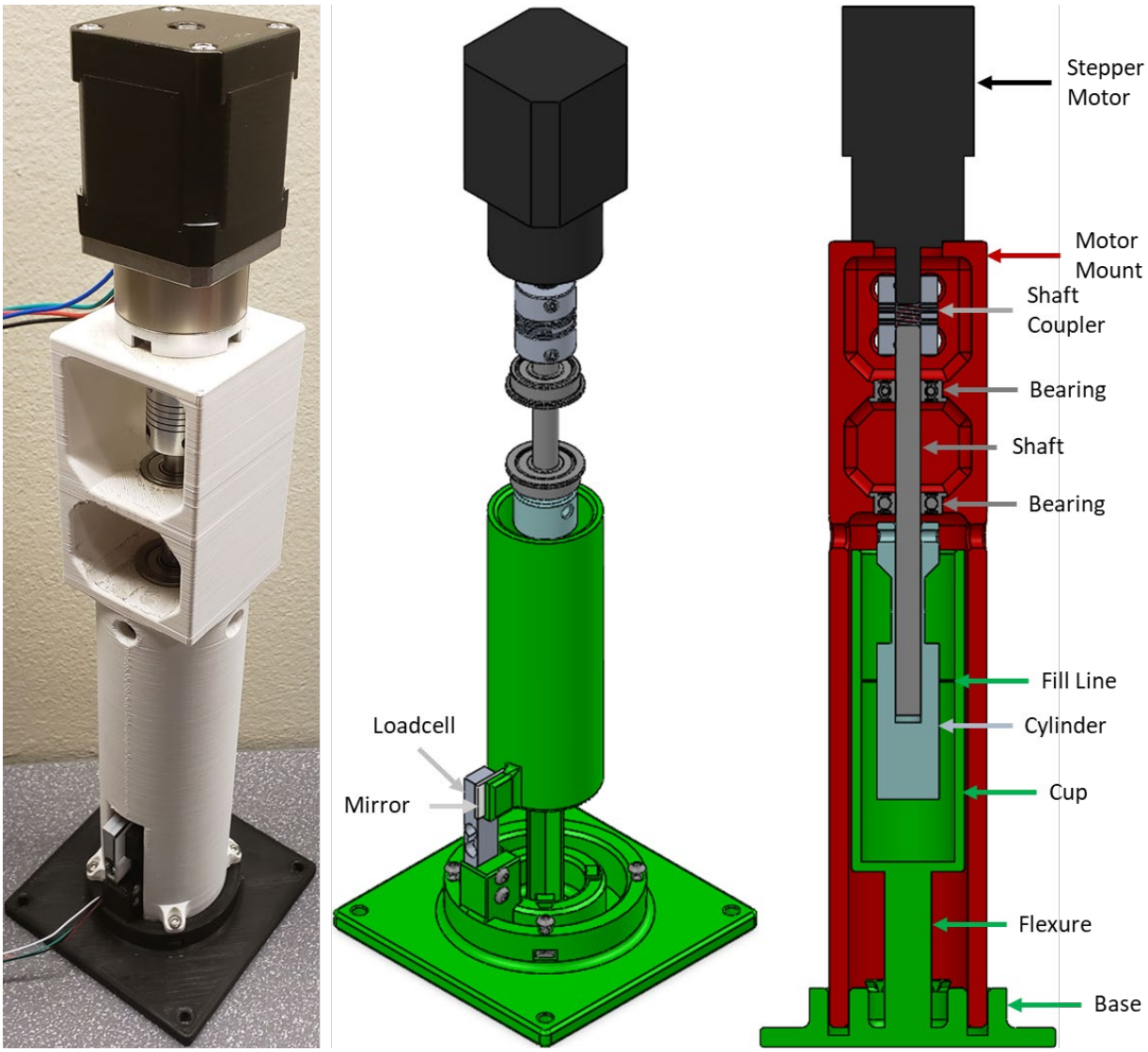

Figure 17: CAD of the version 2 test assembly and a 3D printed prototype. In the CAD, the motor mount is red and the cup-flexure-base component is green. The other components are approximately their actual color. The assembly is approximately 13.1” tall with the motor and 10.2” tall without the motor. The base is a 3.7” square.

4.1 Version 2 Rheometer Design

4.1.1 Drive Train

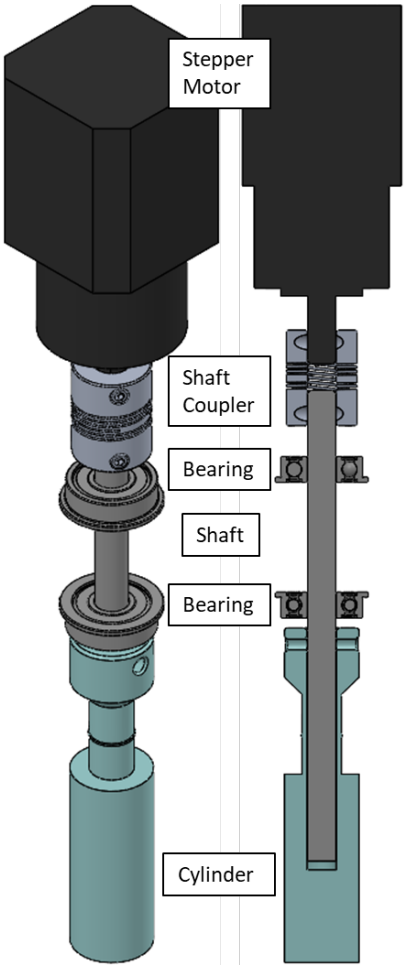

Figure 18: CAD of the version 2 drive train.

As shown in Figure 18, the version 2 design has a few significant differences. A stepper motor was chosen for this design to get a wider usable speed range. Switching to a stepper motor required addressing concerns about non-continuous rotation. To simulate continuous rotation, this setup utilizes a gearbox and is capable of micro stepping [12]. To date, this design has only been tested with 8 micro steps per step due to difficulties interfacing with the stepper controller. Interfacing via software serial communication resulted in inaccurate speeds. To solve this issue so testing could proceed, an Arduino was set to send a signal to the stepper controller indicating when it should step. Despite these complications, this setup was able to achieve a speed range of 60 to 0.25 RPM with the lower limit set by the minimum frequency the Arduino could signal at. To reduce the runout seen in version 1 and since the torque measurement is now decoupled from the drive train, the version 2 design switched from a rigid shaft coupler to a flexible shaft coupler with 2 bearings to reduce the motor's influence on runout. To give this project a wider selection of bearings to choose from, the version 2 design uses an 8mm shaft compatible with the widely available 608 "skateboard" bearings. To assemble the drive train, an assembly aid shown in Figure 19 was designed.

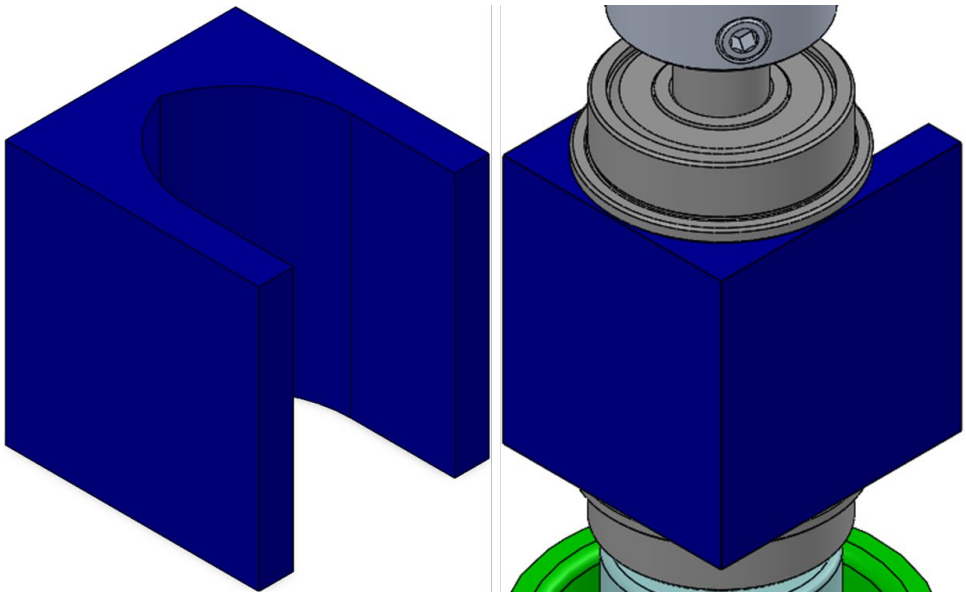

Figure 19: CAD of an assembly aid used to hold the bearings in place while inserting a shaft into the version 2 design.

To assemble the drive train, the bearings are press fit into the motor mount, then the assembly aid in Figure 19 is inserted between the bearings to hold them in place as the shaft is pressed in with an arbor press. This assembly aid was printed as shown with 4 shells and 100% infill to avoid being crushed while installing the shaft.

4.1.2 Loadcell – Flexure Interface

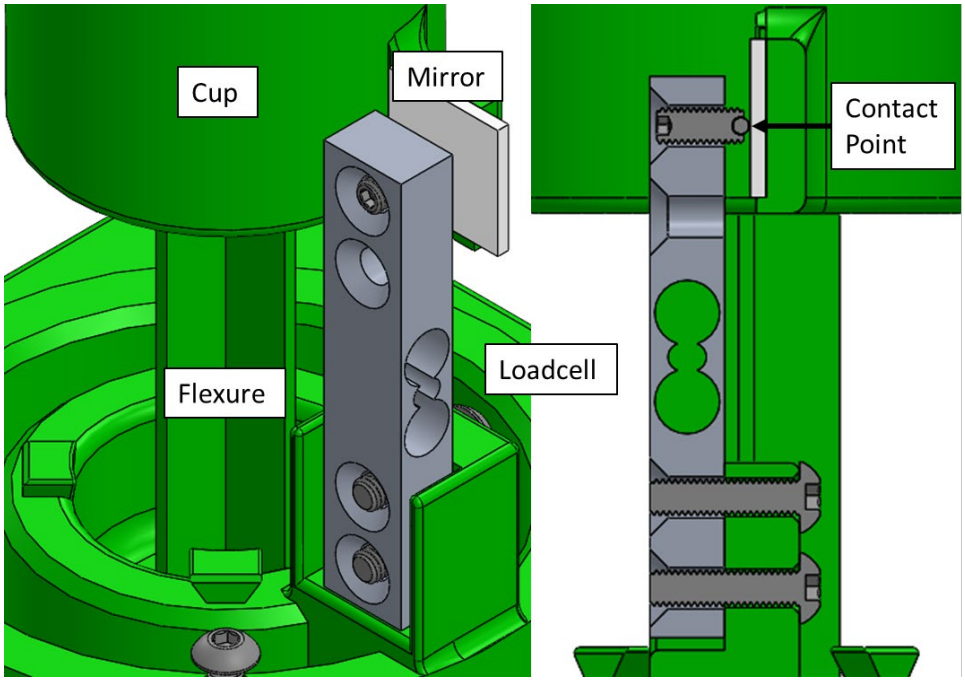

Figure 20: CAD of the interface between the loadcell and the flexure in the version 2 design.

As shown in Figure 20, a ball-point set screw is threaded into the loadcell. It is secured with Loctite so the set screw does not move during testing. The ball interacts with a glass mirror glued to a tab on the cup. The mirror provides a hard surface for the ball to rest against. This design was chosen so there is a well-defined contact point. To ensure they are always in contact, the set screw is tightened an additional half-turn after contacting the mirror to apply a small preload.

4.1.3 Base, Flexure, and Cup

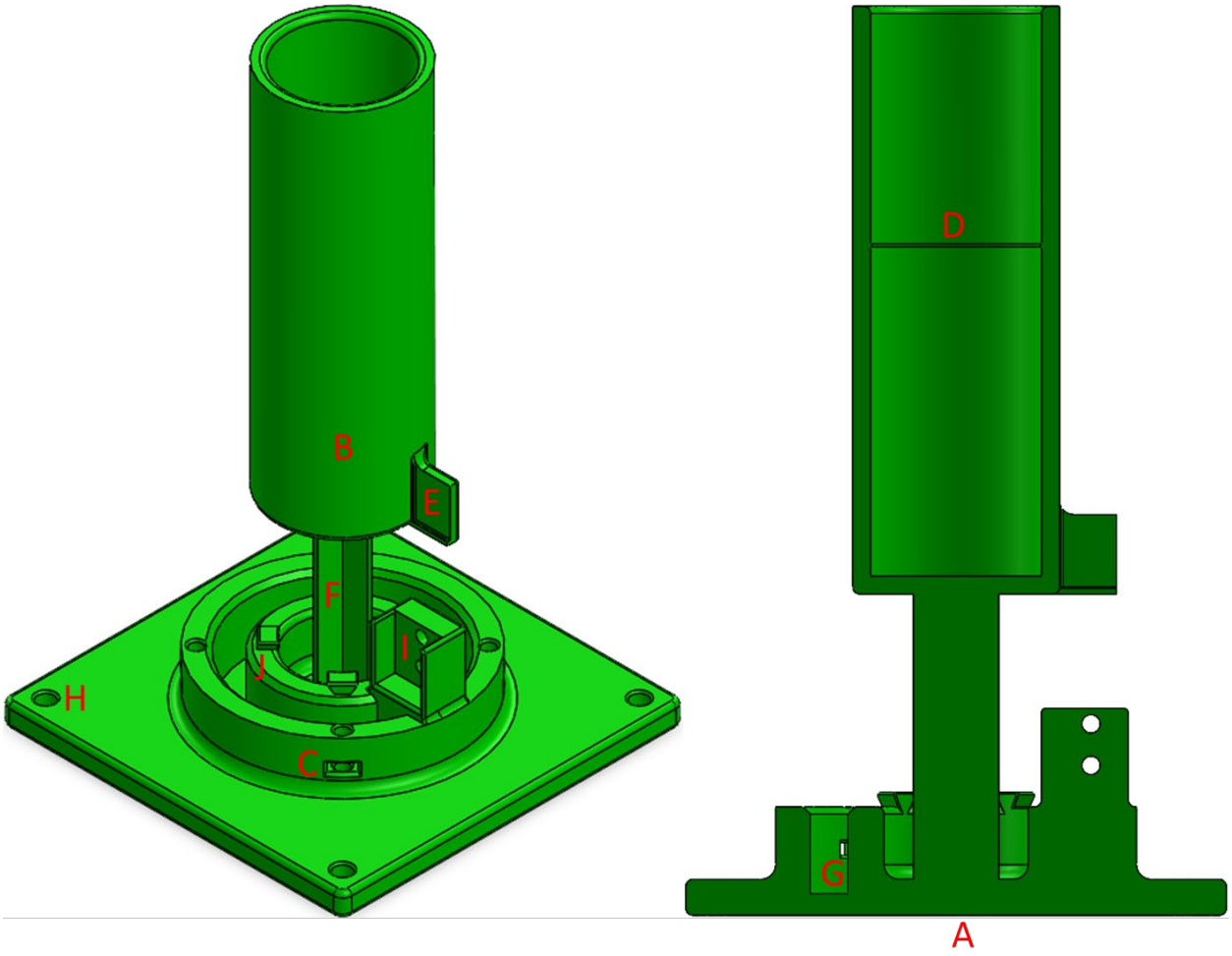

Figure 21: CAD of the version 2 cup-base-flexure component. This part is approximately 6.3” tall by 3.7” square.

As shown in Figure 21, the cup was printed with the bottom surface (A) flat on the print bed to ensure the cup was circular and the cross section of the flexure was symmetrical by printing the cross sections parallel to the x-y plane, 4 shells to prevent leaking, and supports for the cup (B) and the 4 nut slots (C). When generating supports for this structure, it is important to check that none of the supports contact the flexure because that could influence the cross section of the flexure. The cup has a line to mark the fill height (D) and a tab (E) to mount the mirror on and to interface with the loadcell. The tab has small extrusions to position the mirror. The cup is mounted on a plus shaped flexure which can be seen in Figure 22 (F). The base has a slot that the motor mount slides into (G), holes for the 4 sets of nuts and screws (C) to secure the motor mount, and holes for 4 screws (H) to secure the 3D printed base to the wooden base. The base also has a mount

for the loadcell (I). The sides of the loadcell mount were added to reinforce the 3D printed part against bending.

The flexure is fragile, even more so than normal due to it being printed vertically, meaning the layer lines are in the weakest orientation for this part. To protect the flexure when not testing, locks were designed to mount on the 4 dovetail joints (J) on the base. As shown in Figure 22, the locks are designed to slide on and change the cross section of the flexure from a plus sign to a square.

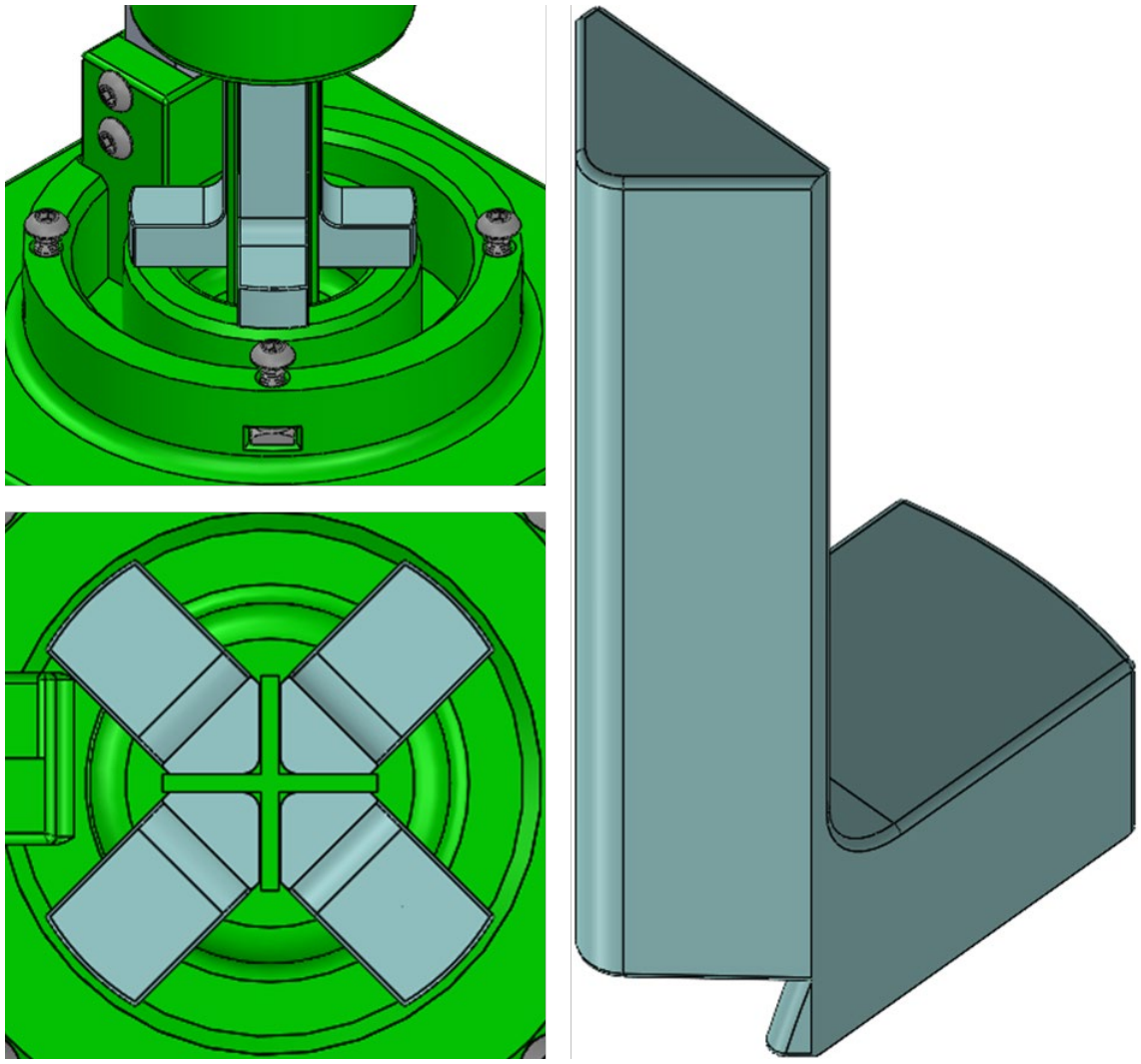

Figure 22: CAD of the version 2 flexure locks showing how they change the cross section.

The fit of the locks is imperfect, so the locks do not entirely prevent the flexure from moving as originally intended, but they support it and limit its range of movement. The cup proved to be waterproof and was able to hold water up to the fill line for 24 hours without leaking or change in water level. The first print was unsuccessful because the supports did not constrain the flexure adequately, so the cup was able to move while being printed which created small layer shifts. To solve this problem, additional supports were added in CAD as shown in Figure 23. The additional supports are designed to be easy to remove with a pair of cutting pliers.

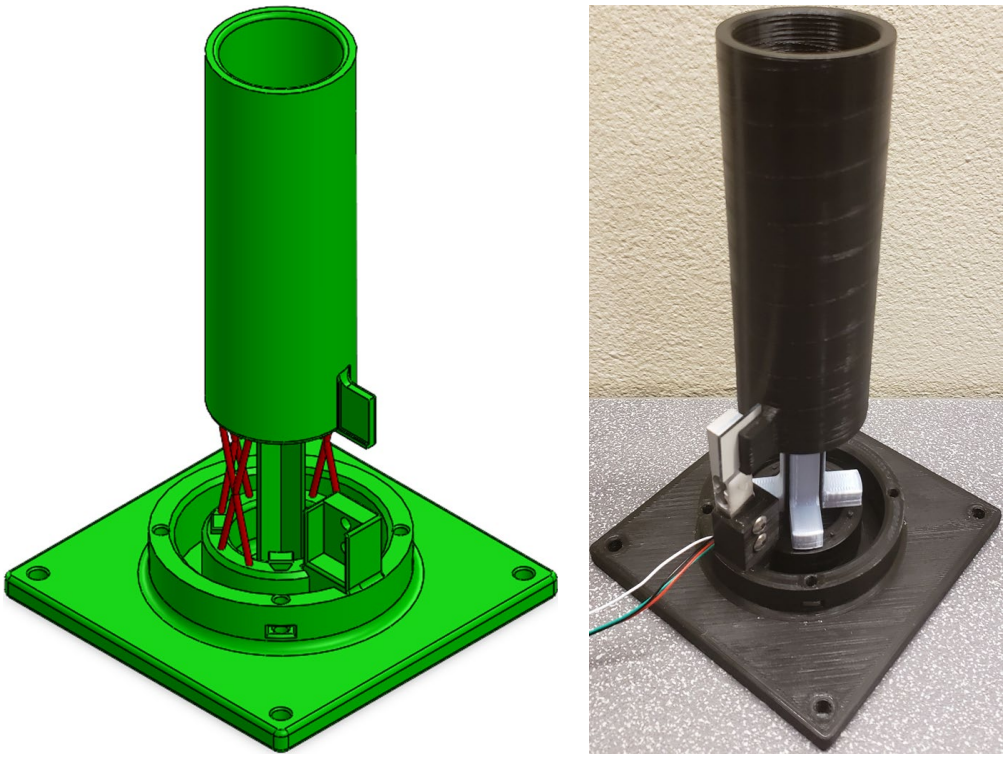

Figure 23: CAD of the version 2 cup with the additional supports for printing the cup shown in red and the 3D printed prototype of the cup, flexure, and base with the locks, loadcell, mirror, and nuts in place and with the supports removed.

The 3D printed prototype is shown in Figure 23. In addition to gluing the mirror in place, the nuts to secure the motor mount are glued in place to prevent them from falling out while cleaning the device. As shown in Figure 24, simple simulations were run in Solidworks to ensure the flexure is at least 10 times less stiff than the loadcell in rotation per advice from Professor Trumper [15].

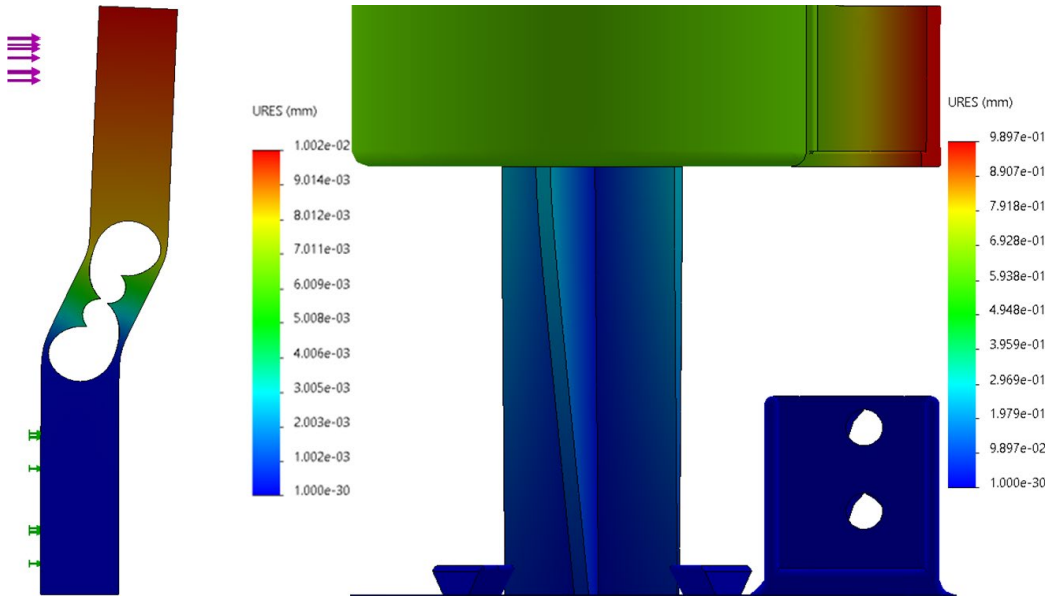

Figure 24: Simulation showing the flexure is about 80 times as flexible as the loadcell.

The simulation in Figure 24 uses a torque of 0.02 Nm on the inside of the cup. This torque is the maximum expected torque from a 10 Pa.s fluid with the cylinder rotating at 100 RPM. This was converted to a 1.3 N force experienced by the loadcell. Under these conditions, the cup rotated a distance of about 0.8 mm at the contact point while the loadcell displaced about 0.01 mm at the contact point.

4.1.4 Motor Mount

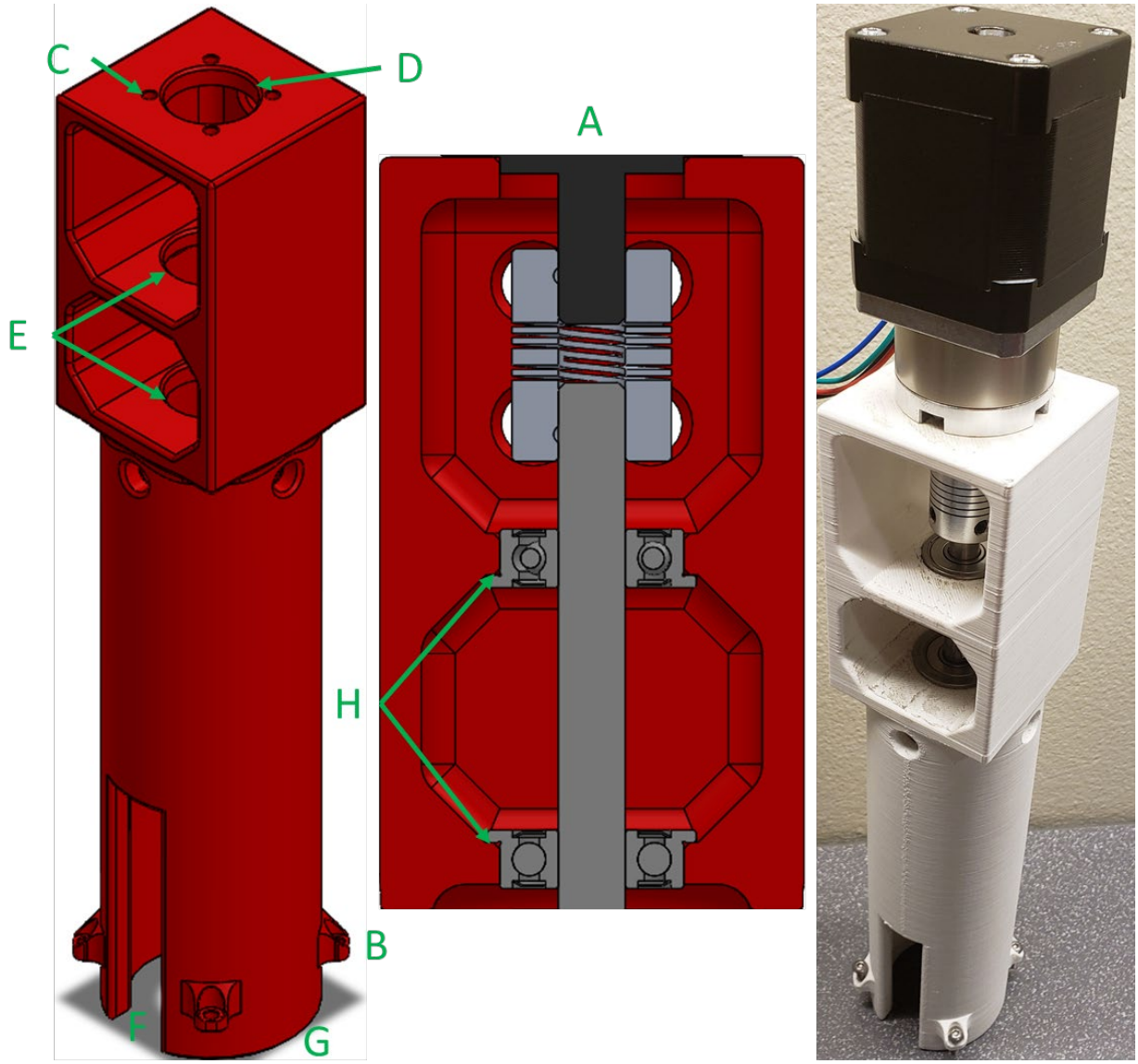

Figure 25: CAD of the version 2 motor mount and a 3D printed prototype. This part is approximately 9.9" tall and is an approximately 2.5" square.

As shown in Figure 25 the motor mount was printed with the top surface (A) flat on the print bed, 2 shells, and supports inside the part and outside for the 4 screw mounts (B). The 8 additional horizontal holes are for tool access and the vertical holes (B (x4) and C (x4)) are for screws, the motor (D), and the 2 bearings (E). The slot cutout at the bottom (F) is to accommodate the loadcell. The chamfers on the 4 screw mounts (B) were added to make the part easier to print. The

cylindrical part below the screw mounts (G) slides into the slot on the cup. The 2 bearings are designed to press fit into the bearing holes (E). To ensure a tight press fit, the 2 holes (E) were printed less than 1mm smaller in diameter then manually reamed out with a 22mm drill bit. It is essential to ensure the bearings are aligned and positioned correctly as the bearings control the concentricity of the shaft. The surfaces the 2 bearing flanges rest against (H) have support material remnants; therefore, post processing is required to make the surface adequately flat. To ensure the bearings are positioned correctly and the shaft is aligned, the surfaces the bearing flanges rest against (H) were milled after printing so the surfaces were free of support material, flat, and parallel.

4.1.5 End Effector Geometries

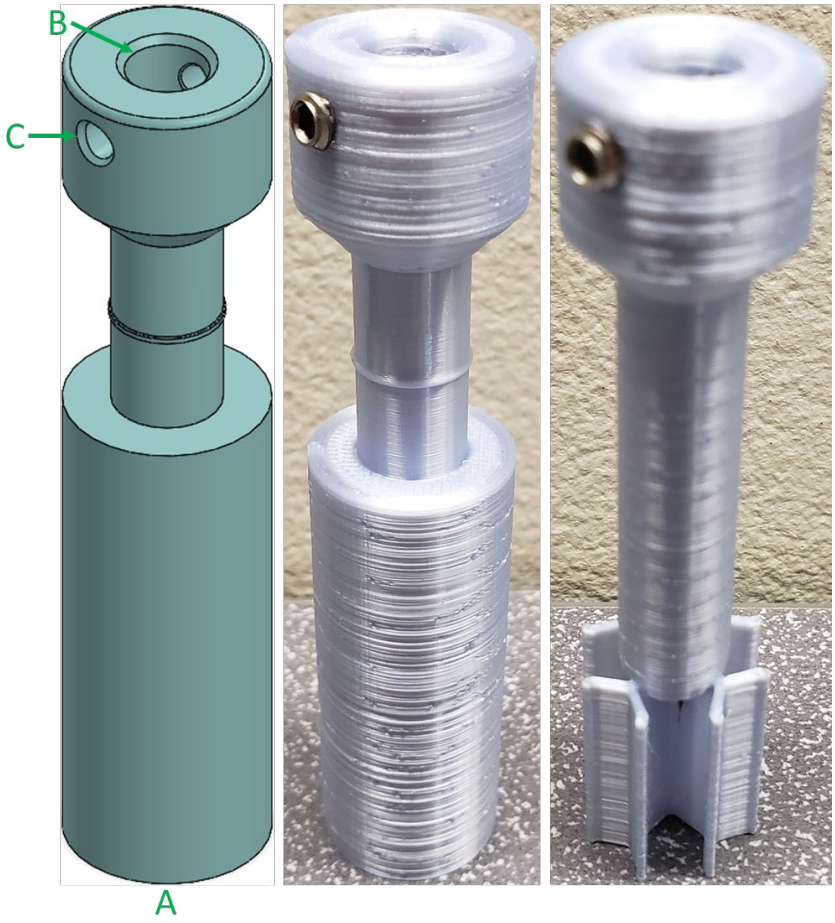

Figure 26: CAD of the version 2 cylinder end effector, a 3D printed prototype, and an alternate vane geometry with 8 vanes. This part is approximately 3.5” tall with a diameter of about 0.8”.

The version 2 cylinder shown in Figure 26 is fundamentally the same as version 1 in Figure 3. The primary difference is that it has a smaller diameter to make concentricity less important as the gap has less weight in Equation 2. It was printed with the bottom surface (A) flat on the print bed, 4 shells to help prevent leaking, and no supports. To give this part extra rigidity, the shaft goes into the hole in the top (B) and 2.5” deep into this part. After printing this hole was reamed to fit the 8mm shaft. The 2 holes (C) are for set screws to secure the part to a shaft and were reamed

and tapped as in version 1. Also shown is an alternate vane geometry with 8 vanes which has not been used in testing yet.

4.1.6 Version 2 Electronics Wiring Diagram

Figure 27 shows the wiring diagram for version 2. The main components are an Arduino Uno, a loadcell amplifier, a loadcell, a stepper controller, and a stepper motor. The Arduino collects the loadcell data and controls the stepper controller which controls the stepper motor.

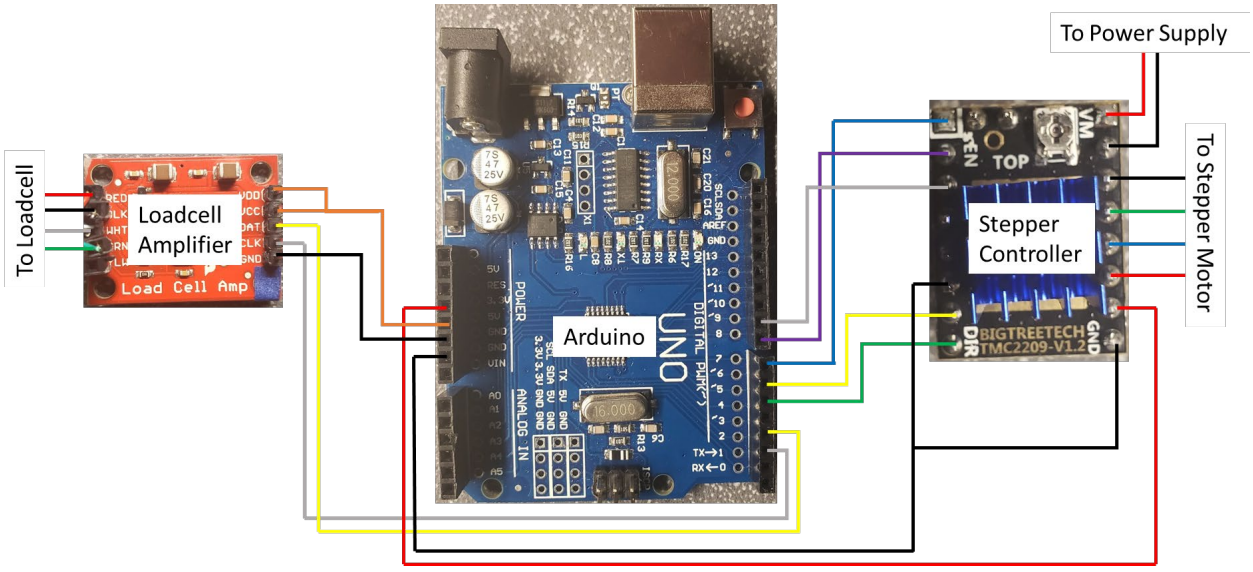

Figure 27: Wiring diagram for version 2. It includes an Arduino Uno, a loadcell amplifier, and a stepper controller. The loadcell and stepper motor are not shown.

4.2 Loadcell Testing and Calibration

To ensure the loadcell was providing linear data, it was tested by hanging weights off it. The loadcell was secured to a base as shown in Figure 28, and using a thin gauge wire, an increasing amount of weight was suspended from the set screw that would normally be in contact with the mirror during viscosity testing.

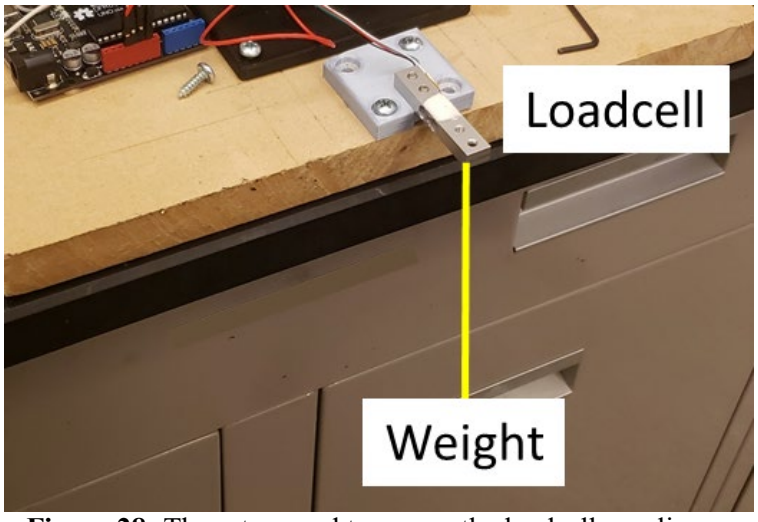

Figure 28: The setup used to ensure the loadcell was linear.

The test was run twice. The first set used weights from 10.6 to 90.6 grams and the second set used weights from 57.43 grams to 257.43 grams. The results are shown in Figure 29.

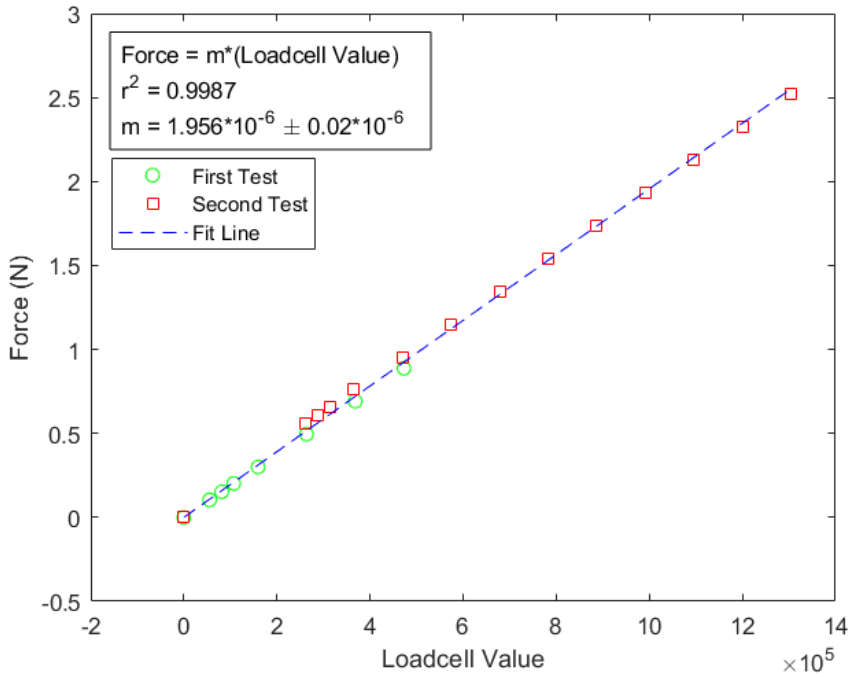

Figure 29: These are the results from hanging increasing amounts of weight on the loadcell and measuring the output of the loadcell. The data was fit with a linear equation of Force = 1.956*10-6*(Loadcell Value).

The fit is nearly perfectly linear, but there is some shifting between the two data sets. This could be caused by a change in environmental noise, temperature, or how the force was transferred to the loadcell between the two tests. To avoid error stack up, instead of using the above tests to calculate the relationship between loadcell values and torque, the conversion equation was found by testing fluids. To accomplish this calibration, the loadcell-cup-flexure-base assembly was attached to a DHR3 rheometer from TA Instruments with double sided tape as shown in Figure 30.

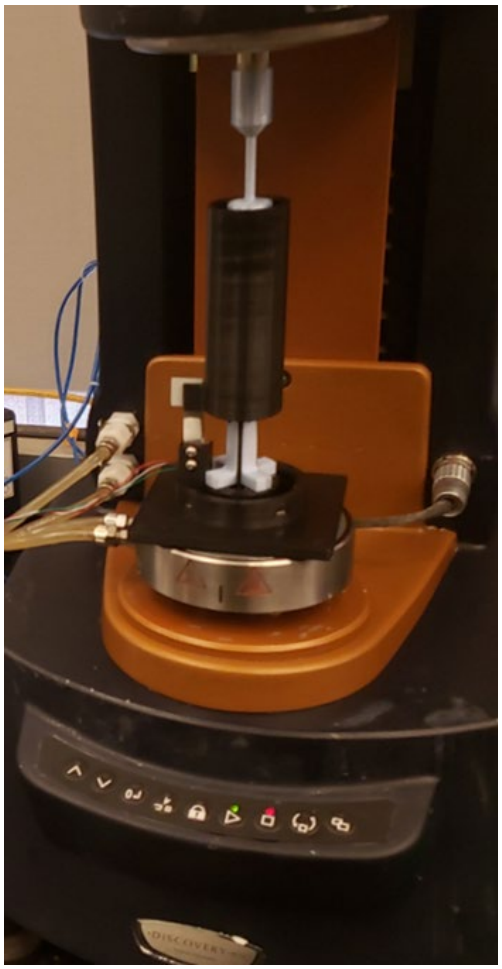

Figure 30: This is the testing setup used to calibrate the loadcell. The locking mechanisms on the flexure were removed before data was taken.

Constant rotation rate tests were conducted with a 0.5 Pa.s calibration fluid at rotation rates of 10, 3.2, 1, 0.32, 0.1, 0.032, and 0.01 radians per second. For both the DHR3 and version 2 of this rheometer, the noise altered the measurement significantly for rotation rates lower than 0.1 radians per second, but the DHR3 continued to have distinguishable steps while version 2 of this rheometer had no distinguishable steps below 0.1 radians per second. To find the conversion equation, each step had the edge effects trimmed off, and the remaining data was averaged. The data is shown in Figure 31 and the results are shown in Figure 32 including a fit line that will be used to convert loadcell values into torque for the rest of Section 4.

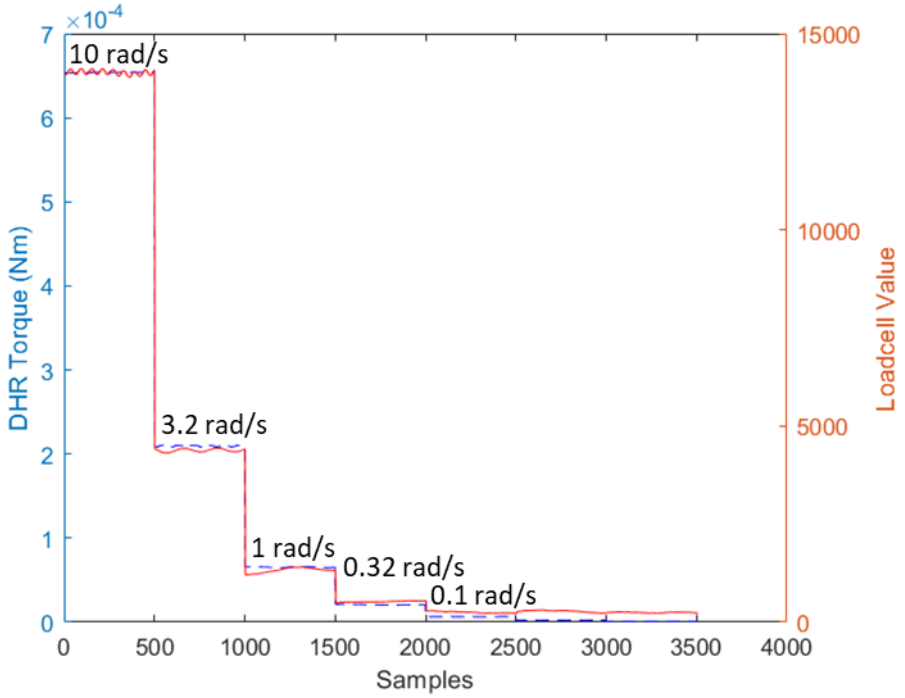

Figure 31: This graph shows the DHR torque and loadcell value step functions from testing a 0.5 Pa.s sample.

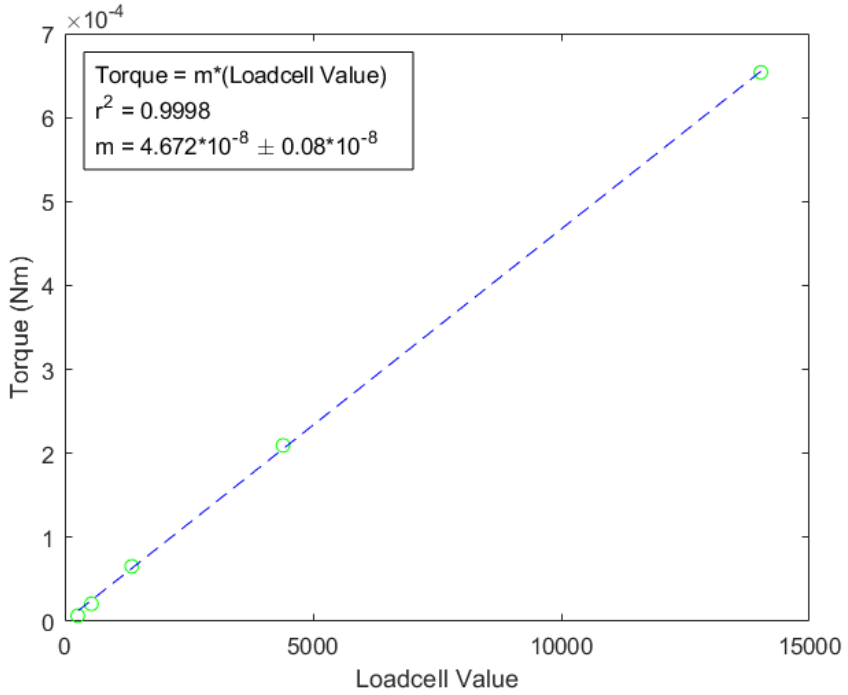

Figure 32: This graph compares the torque read by the DHR3 to the loadcell values from the loadcell on version 2. The fit line has an equation of Torque = $4.672*10^{-8}$*(Loadcell Value). The rotation rate intervals were chosen to give a consistent spacing on a log scale.

This conversion equation is not significantly different from the one found by hanging weights off the loadcell. From hanging weights off the loadcell the slope is $4.586*10^{-8} \pm 0.05*10^{-8}$ Nm/Loadcell Value while the slope from testing with the DHR is $4.672*10^{-8} \pm 0.08*10^{-8}$ Nm/Loadcell Value. Equation 7, with Torque in Nm, from the DHR loadcell calibration testing will be used for analysis since it accounts for manufacturing and assembly variations in the lever arm to the loadcell.

$$Torque = 4.672 \cdot 10^{-8} \cdot (Loadcell\ Value) \tag{7}$$

4.3 Version 2 Viscosity Testing: Methods, Results, and Discussion

With the setup shown in Figure 33, 6 fluids were tested: 10, 1, 0.5, and 0.1 Pa.s viscosity standards as well as hand sanitizer and shaving foam. The viscosities from these tests were found using Equations 1, 2, and 3 with rotation rate and loadcell data as well as Equation 7 from the loadcell calibration testing.

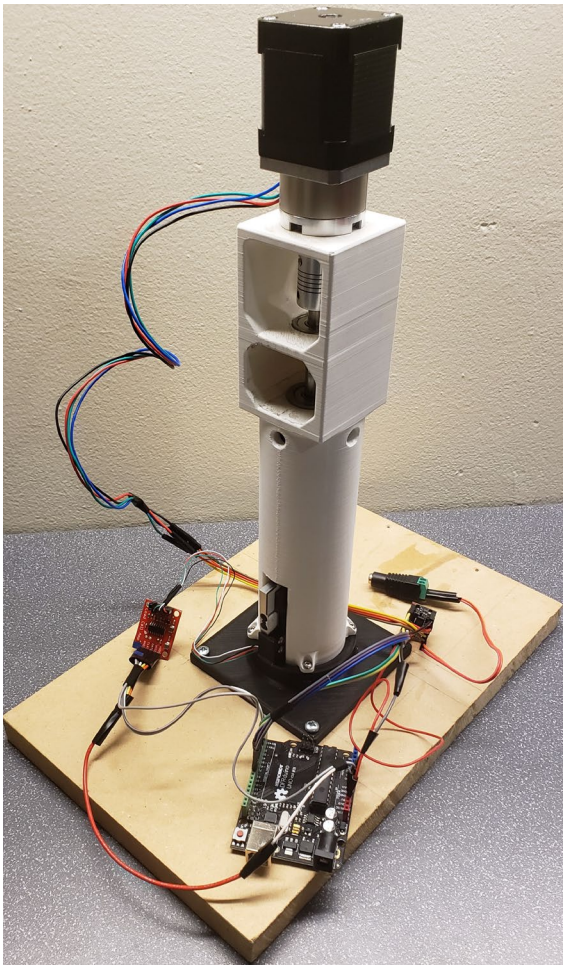

Figure 33: This is the setup used for testing.

To test a fluid with version 2, the base is secured to a larger base such as the block of wood in Figure 33, then the fluid under test is filled up to or slightly above the fill line on the cup before removing the flexure locks and screwing the motor mount to the 3D printed base. During testing, the ambient temperature is measured because the viscosities are temperature dependent.

The temperature was found to be around 19°C and the sample viscosity values were adjusted or measured for 19°C. For a testing cycle, the code, similar to that in Appendix C, tares the loadcell then ramps the motor up to 60 RPM before running through up to 5 different speeds per decade between 60 and 0.25 RPM, staying at each speed for 15 seconds and moving from high speed to low speed. Only 9 seconds of the 15 seconds of data are used for the viscosity calculations because the first 5 seconds and last second of each speed are removed to ensure the sample is at steady state and to avoid bad data from speed changing. Some tests with lower viscosity samples did not produce a step function and gave unusable data. This could have been caused by variations in environmental noise or the motor performance changing with temperature. Figure 34 shows the raw data, omitting the ramp up to speed, from the loadcell for a test with a 10 Pa.s liquid.

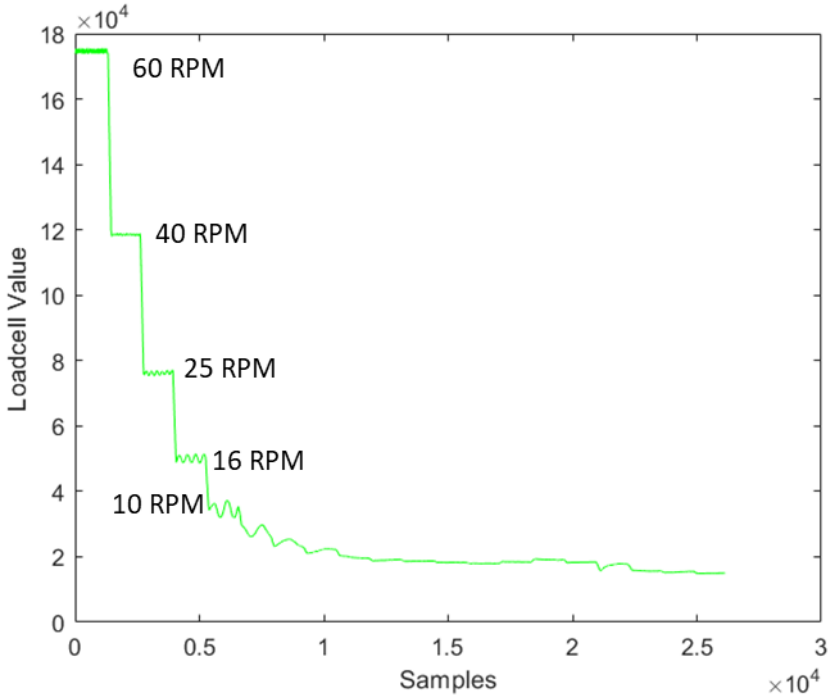

Figure 34: This shows the raw loadcell data for a test run in 10 Pa.s fluid.

Ideally the loadcell value should be a step function, and except for some oscillations, it is at and above 10 RPM. Figure 35 zooms into the oscillation on the first step, at a rotation rate of 60 RPM. One datapoint sample takes approximately 10 ms.

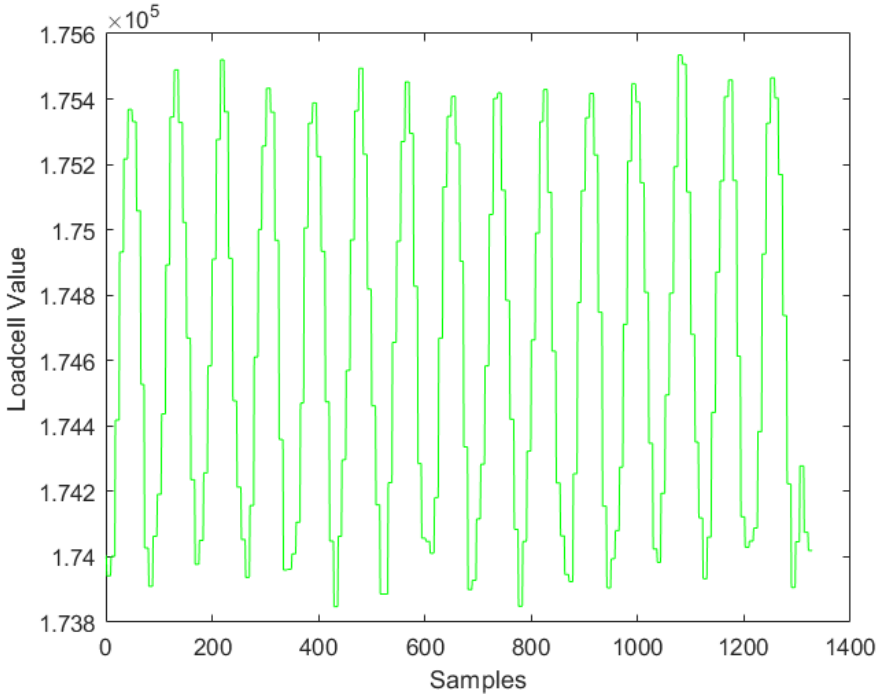

Figure 35: This shows the oscillations at 60 RPM in a 100 Pa.s fluid.

The oscillation frequency of approximately 1 Hz correlates with the motor rotation frequency of 1 rotation per second at 60 RPM. The oscillations in the other steps also happen once per rotation. These oscillations are likely due to small eccentricities in the drive train and cup. Due to the oscillations, data collected for speeds slower than 6.7 RPM is less reliable because slower speeds do not complete a full rotation during the 9 seconds of data that are analyzed and the small torque values could be obscured by the oscillations. Based on this, speeds lower than 6.7 RPM were omitted from the viscosity analysis. It is also possible that the unreadable data is caused by the stepper not rotating smoothly enough at small rotation rates with 8 micro steps per step. Figure 36 shows the results for the 4 constant viscosity samples.

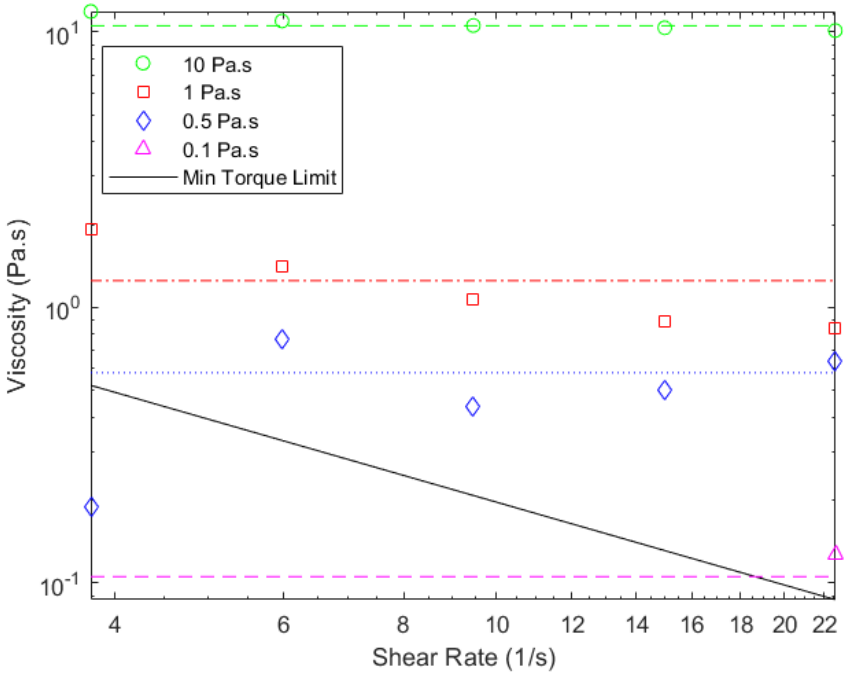

Figure 36: This figure shows the viscosity vs shear results for the 4 constant viscosity samples: 10, 1, 0.5, and 0.1 Pa.s. The points show the data collected using version 2, and the lines show the expected results [16, 17]. The black line shows the practical minimum torque limit which was found to be approximately $7*10^{-5}$ Nm.

Sample Name	Actual Viscosity (Pa.s)	Average Measured Viscosity (Pa.s)	Average Percent Difference (%)	Max Percent Difference (%)
10 Pa.s	10.55	10.78	-2.2	-12.6
1 Pa.s	1.25	1.23	1.6	-52.8
0.5 Pa.s	0.58	0.51	12.1	-67.2
0.1 Pa.s	0.11	0.13	-18.2	-18.2

Table 1: Compilation of the results from the tests shown in Figure 36 quantitatively showing the accuracy of version 2. The actual viscosities for the 10 Pa.s and 0.1 Pa.s samples are based on the datasheet and adjusted for 19°C while the 1 Pa.s and 0.5 Pa.s samples were measured with the DHR3 at 19°C to find the actual viscosities [16, 17].

Table 1 shows the results from testing and lists the percent differences between the actual and measured viscosities. The percent difference between the actual viscosity and the average measured viscosity was within 18.2%, but individual points could vary as much as 67.2% from the actual value. The 0.1 Pa.s sample only has one data point because for speeds lower than 40 RPM, the torque value could not be differentiated from the system noise. The variations in the data likely come from variations in noise due to the previously mentioned oscillations: if an integer number of rotations were completed during the timespan analyzed. Figure 37 shows the shear stress vs shear rate results for the 4 constant viscosity samples, and Figure 38 shows the Reynolds number vs viscosity results for the 10 and 0.1 Pa.s samples.

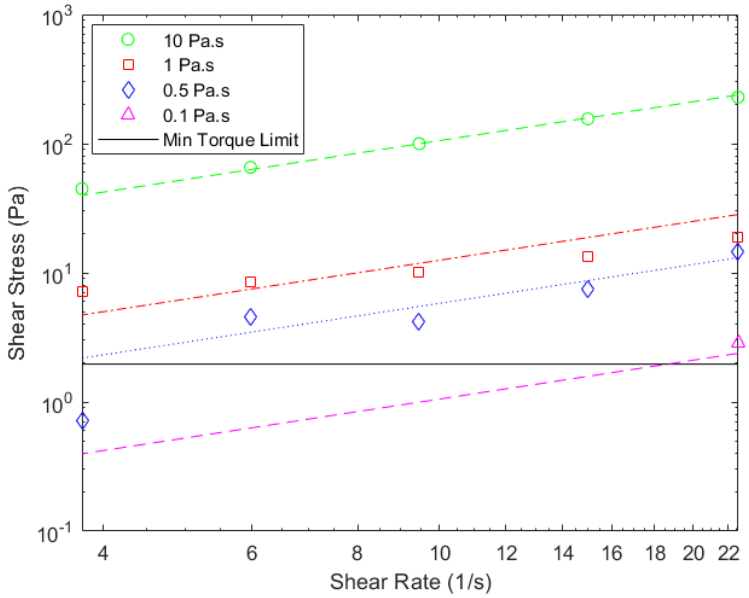

Figure 37: This figure shows the shear stress vs shear rate results for the 4 constant viscosity samples: 10, 1, 0.5, and 0.1 Pa.s. The points show the data collected using version 2, and the lines show the expected results [16, 17]. The black line shows the practical minimum torque limit which was found to be approximately $7*10^{-5}$ Nm.

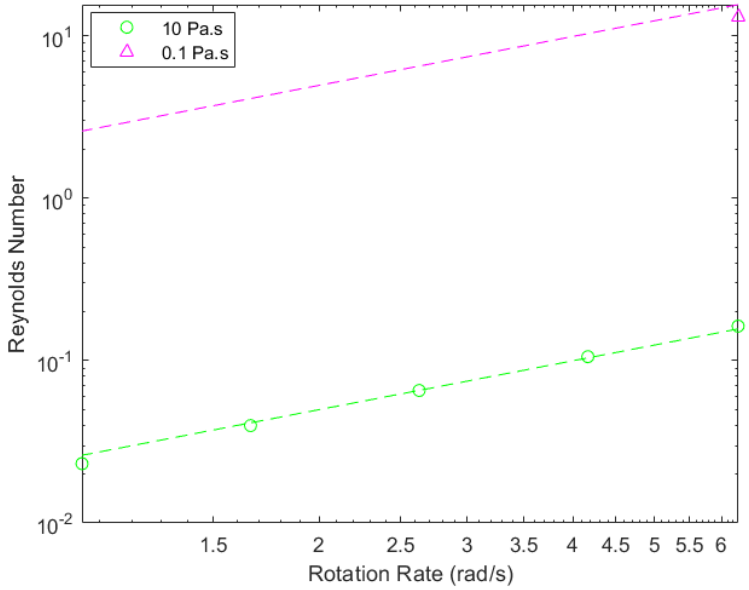

Figure 38: This figure shows the Reynolds number vs rotation rate results for 2 constant viscosity samples: 10 and 0.1 Pa.s. The points show the data collected using version 2, and the lines show the expected data [16, 17]. Equation 4 was used to find the Reynolds number.

Only 10 and 0.1 Pa.s results are shown in Figure 38 as the densities of the other samples could not be found on their datasheets and were not recorded during testing. Figure 39 shows the viscosity vs shear rate results for hand sanitizer.

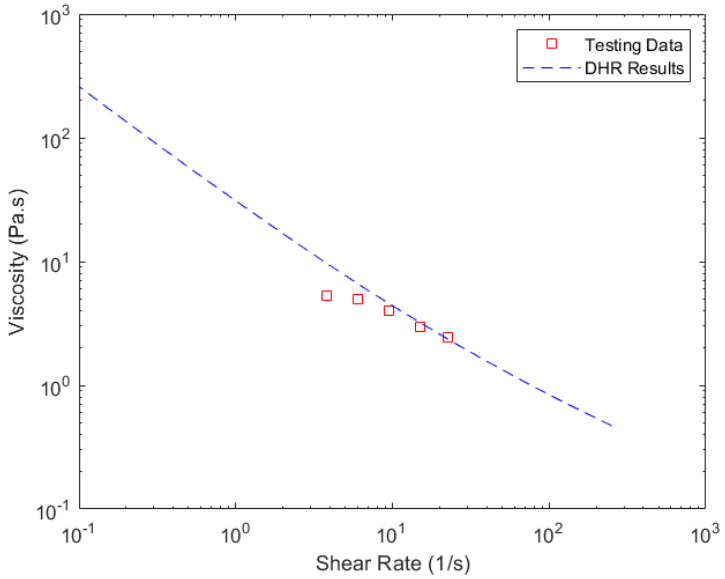

Figure 39: This figure shows the viscosity vs shear rate results for hand sanitizer. The points show the data from version 2, and the line shows the comparison data from the DHR3 rheometer.

Noise in the system skewed the averages for the slower shear rates, but for the measurable shear rate range, some of the data is still close to the actual curve measured by the DHR3 with one data point being within 3.9%, but others can vary as much as 42.6%. Figure 40 shows the shear stress vs shear rate results for hand sanitizer.

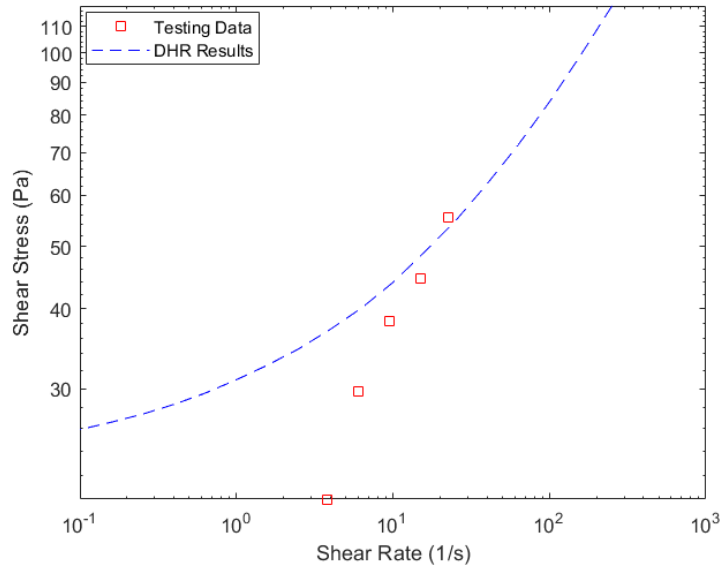

Figure 40: This figure shows the shear stress vs shear rate results for hand sanitizer. The points show the data from version 2, and the line shows the comparison data from the DHR3 rheometer.

The shear stress vs shear rate data in Figure 40 shows similar deviation from the expected curve as was found with the viscosity data. These deviations could be caused by the sample slipping against the cup and cylinder geometry. Figure 41 shows a better result for shaving foam.

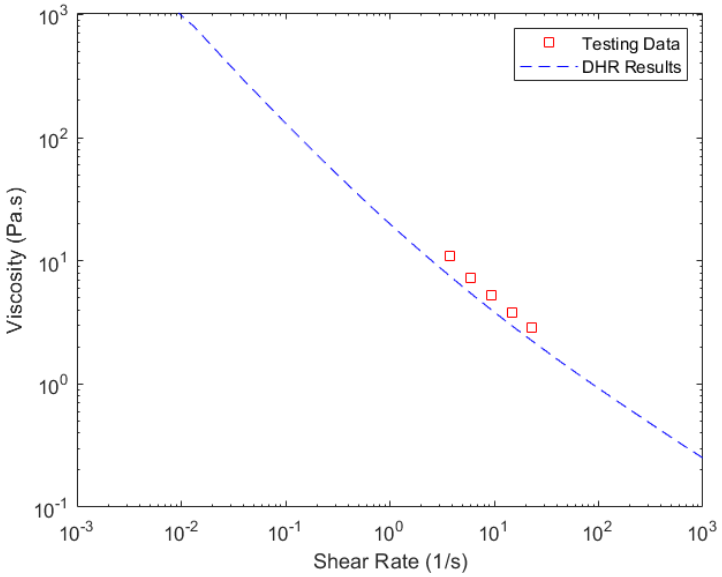

Figure 41: This figure shows the viscosity vs shear rate results for shaving foam. The points show the data from version 2, and the line shows the comparison data from the DHR3 rheometer.

Unlike the hand sanitizer, the data for the shaving cream has nearly the same curve as the DHR3 results, but with a small offset. The spread of the variation in the data is much smaller with all but 1 datapoint being within 35 to 38% of the curve from the DHR3 results, but the last data point has a percent difference of 50.6% from the actual curve. The shift in the data could be caused by a shift in the environmental noise after the loadcell was tared. Figure 42 shows that the shear stress vs shear rate results for shaving foam also follow the DHR3's curve with a small offset.

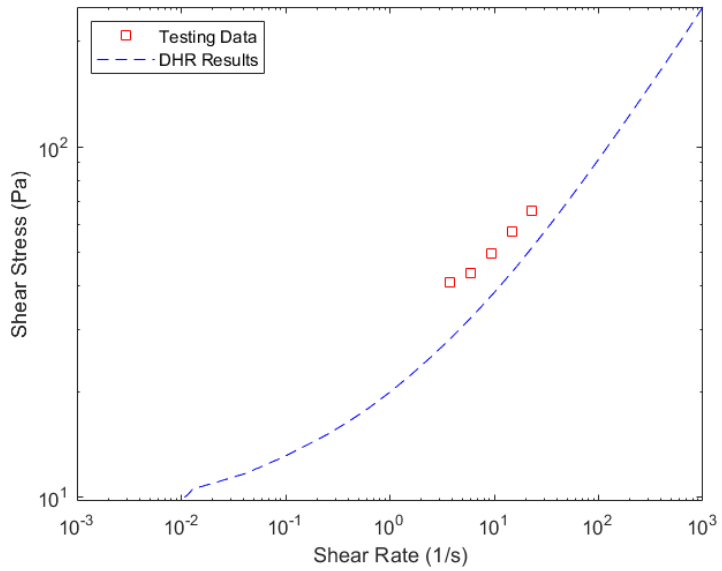

Figure 42: This figure shows the shear stress vs shear rate results for shaving foam. The points show the data from version 2, and the line shows the comparison data from the DHR3 rheometer.

5. Conclusion and Future Work

The goal of this work was to prove that this design concept could become a functional rheometer and to find the areas of the design most in need of improvement. This was successfully accomplished by showing that this device could measure viscosities between 10 and 0.1 Pa.s with the average being within 18.2% of the actual values. This device was also able to measure two shear-thinning fluids with an accuracy of within 50.6%. Table 2 compares the desired basic specifications to those demonstrated with the designs in this paper. A future version of this design could prove to be a cheaper, more customizable replacement for more expensive rheometers such as the DHR3 used to verify the measurements.

	Desired	Version 1 Rheometer	Version 2 Rheometer
Speed Range (RPM)	0.01 – 100	20 – 90	0.25 – 60
Viscosity Range (Pa.s)	0.01 – 10	100	0.1 – 10
Min Measurable Torque Limit (Nm)	10^{-5}	$7*10^{-2}$	$7*10^{-5}$
Max Cost ($)	200	150	200

Table 2: Comparison of the desired specifications with the tested capabilities of the rheometer designs in this paper. The version 1 rheometer only has a single value listed for the viscosity range because of the samples tested it was the only sample with readable data, but no samples above 100 Pa.s or between 10 and 100 Pa.s were tested.

5.1 Future Work

There are 2 major issues that need to be improved for this to be a functional and practical rheometer: the noise and the usability. The noise comes in 2 parts: the electrical and the mechanical. While electrical noise seems to have only been a minor component of the noise, it is still best practice to take a few simple countermeasures to prevent it from affecting future measurements. To minimize the electrical noise, any wires carrying analog signals, such as the wires for the loadcell, should be trimmed as short as is reasonable and shielded with the shielding grounded. Ferrite beads can also be added to the wires to further reduce noise.

To minimize the mechanical noise, both the runout and vibrations in the system need to be improved. A window should be added to the shield on the motor mount so the runout of the drivetrain can be measured with a dial indicator. It may also be useful to test parts where the bearing holes in the motor mount and the shaft hole in the cylinder are machined on a lathe. To improve the vibrations, a stepper motor without a gearbox should be tested and the finest usable micro stepping setting should be used for each rotation rate to ensure the smoothest possible rotation. The stepper motor should also be mounted using rubber washers or another method that will increase the isolation of the system from the motor's vibrations. Similarly, the system should be mounted or set on something such as a foam pad to limit the influence of environmental noise. To further limit the impact of environmental noise, the loadcell and flexure should be enclosed while collecting data.

Currently, the version 2 design utilizes a few large parts to limit error stack up from assembling the parts, but the final design must be printable on smaller 3D printers and should have smaller print times reducing the cost of 3D printing replacement parts, especially for the fragile flexure. It should also be possible to wash the cup without taking the flexure and 3D printed base assembly off the wooden base, and common procedures like cleaning the cup will ideally be toolless. To accomplish this, the 3D printed parts should be split into smaller components, but this

needs to be done carefully and gradually as it could increase the noise in the system. First, the cup and the flexure should be separated. This could be accomplished using a threaded joint similar to that used in the version 1 rheometer.

Second, for ease of printing and assembly, the motor mount should be separated into 3 pieces: a plate the stepper mounts onto, the bearing housing, and the cylindrical extrusion that mounts to the base. The stepper plate can bolt onto the bearing housing. This was not done in version 2 because the design was carried over from version 1 where it was critical that the motor shaft was concentric to the bearing. The bearing housing can connect to the cylindrical extrusion with circular press fit features similar to how the motor mount connected to the cup in version 1 but with the addition of keyed features to constrain rotation. The cylindrical extrusion should also connect to the base in a toolless manner such as with threads similar to how the cup connected to the base in the version 1 rheometer. The cylinder geometry testing attachment is more difficult to add toolless removal to. One possibility is to use a keyed or D shaft and press fit the cylinder onto the shaft. The key or D geometry will constrain rotation, but only the press fit will constrain vertical motion.

Ideally, the flexure would also be separate from the base, but it may be difficult to find a workable method to add that feature in a 3D printed design. With a replaceable flexure it would still be beneficial to experiment with improving the durability of the flexure by testing different reinforcing coatings such as superglue and different printing materials such as PETG, nylon, and Onyx. It may also be useful to experiment with different flexure designs such as the compliant rolling-contact element planetary gear system flexural bearing [18]. While less critical with a replaceable flexure, it would still be best to improve the support provided by the locks, this should be as simple as tuning the dimensions to create a tighter fit, or adding something such as a small spring clamp to hold the locks in place.

6. Appendices

6.1 Appendix A: Version 1 Rheometer Bill of Materials

Component Name	Units Needed	Part Number	Price Per Unit ($)	Total Cost ($)	Procured From
Motor	1	FIT0522	19.90	19.90	Digikey
Motor Controller	1	DRI0039	14.90	14.90	Digikey
Shaft	1	1265K51	23.00	23.00	McMaster-Carr
Bearing	1	57155K479	12.08	12.08	McMaster-Carr
Arduino Uno	2	1738-1228-ND	19.90	39.80	Digikey
Current Sensor	1	4226	9.95	9.95	Digikey
Power Supply	1	KW-0630	14.99	14.99	Amazon
M3 Screw	6	92095A183	0.07	0.41	McMaster-Carr
M3 Nut	4	97258A101	0.20	0.80	McMaster-Carr
Set Screw	6	92311A238	0.07	0.42	McMaster-Carr
Wood Screws	4	91555A101	0.07	0.27	McMaster-Carr
Wood Base Plate	1	2726N13	7.21	7.21	McMaster-Carr
Wires	16	TD-JW-001-05312020	0.05	0.80	Amazon
Filament*	120	B00J0ECR5I	0.02	2.76	Amazon
				$147.28	

Table 3: Bill of materials for the version 1 rheometer to estimate cost per unit. The total cost estimate per unit was $147.28. The actual cost of construction was slightly higher because in some cases, products were only available in larger quantities than needed. Some components such as the wires are not the components used in the construction of the design, but merely similar placeholders to estimate the cost as some of the components used in the construction of the design were on-hand.

*Grams were used as the units for estimating the cost of the filament used.

6.2 Appendix B: Version 2 Rheometer Bill of Materials

Component Name	Units Needed	Part Number	Price Per Unit ($)	Total Cost ($)	Procured From
Stepper Motor	1	17HS19-1684S-PG5	40.05	40.05	Amazon
Stepper Controller	1	BIQU-UUU001791	6.20	6.20	Amazon
Shaft Coupler	1	XW-190103-01	2.70	2.70	Amazon
Shaft	1	1265K64	23.00	23.00	McMaster-Carr
Bearing	2	57155K631	13.89	27.78	McMaster-Carr
Loadcell	1	B07NRVML17	10.49	10.49	Amazon
Loadcell Amplifier	1	SEN-13879	9.95	9.95	Amazon
Mirror	1	CRDIY	0.08	0.08	Amazon
Ball-Point Set Screw	1	93339A246	7.28	7.28	McMaster-Carr
Arduino Uno	1	1738-1228-ND	19.90	19.90	Digikey
Power Supply	1	SNT2403BK	14.99	14.99	Amazon
M3 Screw	10	92095A183	0.07	0.68	McMaster-Carr
M3 Nut	4	97258A101	0.20	0.80	McMaster-Carr
Set Screw	2	92311A238	0.07	0.14	McMaster-Carr
Wood Screws	4	91555A101	0.07	0.27	McMaster-Carr
Wood Base Plate	1	2726N13	7.21	7.21	McMaster-Carr
Wires	21	TD-JW-001-05312020	0.05	1.05	Amazon
1.75mm PLA Filament*	461	B00J0ECR5I	0.02	10.60	Amazon
				$183.16	

Table 4: Bill of materials for the version 2 rheometer to estimate cost per unit. The total cost estimate per unit was $183.16. The actual cost of construction was slightly higher because in some cases, products were only available in larger quantities than needed. Some components such as the wires are not the components used in the construction of the design, but merely similar placeholders to estimate the cost as some of the components used in the construction of the design were on-hand.

*Grams were used as the units for estimating the cost of the filament used.

6.3 Appendix C: Version 2 Testing Arduino Code

```
#include <TMCStepper.h>                         // Stepper controller library
#include <HX711_ADC.h>                          // Load cell library

#define EN_PIN          7                       // TMC2209 enable pin
#define DIR_PIN         6                       // TMC2209 direction pin
#define STEP_PIN        5                       // TMC2209 step pin
#define MS1             8                       // TMC2209 micro stepping pin
#define MS2             9                       // TMC2209 micro stepping pin

const int HX711_dout = 3;                       // HX711 dout pin
const int HX711_sck = 2;                        // HX711 sck pin

HX711_ADC LoadCell(HX711_dout, HX711_sck);      // Define load cell

float Interval = 15000;                         // Sets the duration of each speed setting
int32_t Speed;                                  // Speed variable
unsigned long StartMillis;                      // Baseline counter variable
unsigned long Time;                             // Current time counter variable
float RPM = 0;                                  // RPM variable

void setup() {
  pinMode(EN_PIN, OUTPUT);                      // TMC2209 Enable pin output
  pinMode(STEP_PIN, OUTPUT);                    // TMC2209 Step pin output
  pinMode(DIR_PIN, OUTPUT);                     // TMC2209 Direction pin output
  pinMode(MS1, OUTPUT);                         // TMC2209 Step pin output
  pinMode(MS2, OUTPUT);                         // TMC2209 Direction pin output
  digitalWrite(EN_PIN, LOW);                    // TMC2209 Enable driver in hardware
  digitalWrite(DIR_PIN, LOW);                   // TMC2209 Set stepper direction
  digitalWrite(MS1, LOW);                       // TMC2209 Set micro stepping
  digitalWrite(MS2, LOW);                       // TMC2209 Set micro stepping

  Serial.begin(2000000);                        // Start serial output

  LoadCell.begin();                             // Start loadcell
  unsigned long stabilizingtime = 2000;         // Set tare time
  boolean _tare = true;                         // Enable tare
  LoadCell.start(stabilizingtime, _tare);       // Reset the scale to 0

  StartMillis = millis();                       // Start time

void loop() {
  Time = millis() - StartMillis;                    // Test Time

  if (Time <= 2*Interval && RPM < 60) {             // Ramp up to speed
     RPM = RPM + 0.1;
   }
  if (2*Interval < Time && Time < 3*Interval) {     // 60 RPM for Interval
    RPM = 60;
  }
  if (3*Interval < Time && Time < 4*Interval) {     // 40 RPM for Interval
```

```
  RPM = 39.811;
 }
```

Lines 68-104 omitted for brevity. They are if loops for Intervals 4 to 12 for rotation rates from 25.12 to 0.63 RPM.

```
 if (13*Interval < Time && Time < 14*Interval) {        // 0.4 RPM for Interval
  RPM = 0.39811;
 }
 if (14*Interval < Time && Time < 15*Interval) {        // 0.3 RPM for Interval
  RPM = 0.25119;
 }
 if (Time > 22*Interval) {                             // End of the test. Turn the motor off.
  RPM = 0;
  digitalWrite(EN_PIN, HIGH);                          // Disable stepper driver
 }

 Speed = round((RPM/60.000000)*(200*5.18*8));          // Calculates the rotation rate
 tone(STEP_PIN, Speed);                               // Sets the PWM frequency which sets the speed

 LoadCell.update();                                   // Updates the loadcell value

 Serial.print(Speed*60/(200*5.18*8));                 // Prints the rotation rate in RPM
 Serial.print(", ");                                  // Comma space to easily split data in Excel
 Serial.println(LoadCell.getData());                  // Prints the load cell value

 delay (10);
}
```

7. References

[1] Owens, C. E., Hart, A. J., and McKinley, G. H., 2020, "Improved Rheometry of Yield Stress Fluids Using Bespoke Fractal 3D Printed Vanes," Journal of Rheology, **64**(3), pp. 643–662.

[2] "The Viscosity of Hand Sanitisers - Perception, Performance and Packaging," Rheology Lab [Online]. Available: https://www.rheologylab.com/articles/household/hand-sanitisers/. [Accessed: 26-Jan-2022].

[3] Azad, M. A., Olawuni, D., Kimbell, G., Badruddoza, A. Z. M., Hossain, Md. S., and Sultana, T., 2020, "Polymers for Extrusion-Based 3D Printing of Pharmaceuticals: A Holistic Materials–Process Perspective," Pharmaceutics, **12**(2), p. 124.

[4] Nofar, M., Salehiyan, R., and Sinha Ray, S., 2019, "Rheology of Poly (Lactic Acid)-Based Systems," Polymer Reviews, **59**(3), pp. 465–509.

[5] Boyes, W., "Instrumentation Reference Book (4th Edition)" [Online]. Available: https://app.knovel.com/kn/resources/kpIRBE0016/toc?kpromoter=federation. [Accessed: 26-Jan-2022].

[6] "Chapter Two: Situational Problems in MPD.: EBSCOhost" [Online]. Available: https://web.p.ebscohost.com/ehost/pdfviewer/pdfviewer?vid=2&sid=3bd8fba4-826e-459a-bb53-125049fa145d%40redis. [Accessed: 05-Feb-2022].

[7] Durst, F., Arnold, I., and Durst, F., 2008, *Fluid Mechanics: An Introduction to the Theory of Fluid Flows;* Springer, Berlin Heidelberg.

[8] News, P. I., "Measuring Viscosity Wirelessly," Petro Online [Online]. Available: https://www.petro-online.com/news/measurement-and-testing/14/sensor-technology-ltd/measuring-viscosity-wirelessly/50976. [Accessed: 26-Jan-2022].

[9] Hearn, E. J., 1997, Mechanics of Materials: An Introduction to the Mechanics of Elastic and Plastic Deformation of Solids and Structural Materials, Butterworth-Heinemann, Oxford ; Boston.

[10] Rabani, A., and Challis, R., 2013, "A Low-Cost Viscometer Based on a Permanent Magnet Dc Motor," Meas. Sci. Technol., **24**(3), p. 035304.

[11] Hopkins, J. B., and Culpepper, M. L., 2010, "Synthesis of Multi-Degree of Freedom, Parallel Flexure System Concepts via Freedom and Constraint Topology (FACT) – Part I: Principles," Precision Engineering, **34**(2), pp. 259–270.

[12] Mitra, D, "How to Improve Motion Smoothness and Accuracy of Stepper Motors," TI [Online]. Available: https://www.ti.com/lit/an/sloa293a/sloa293a.pdf. [Accessed: 26-Jan-2022].

[13]

Collins, D., 2017, “Microstepping for Stepper Motors,” Linear Motion Tips [Online]. Available: https://www.linearmotiontips.com/microstepping-basics/. [Accessed: 26-Jan-2022].

[14] Vasquez, J., 2021, “Sanity Check Your Engines With This Dynamometer,” Hackaday [Online]. Available: https://hackaday.com/2021/04/14/sanity-check-your-engines-with-this-dynamometer/#more-470834. [Accessed: 26-Jan-2022].

[15] Trumper, D., Jan 4, 2022. “Re: Thesis Project.” [email].

[16] “Polydimethylsiloxane, Trimethylsiloxy Terminated, 10,000 CSt,” Gelest, Inc [Online]. Available: https://www.gelest.com/product/DMS-T41/. [Accessed: 26-Jan-2022].

[17] “Polydimethylsiloxane, Trimethylsiloxy Terminated, 100 CSt,” Gelest, Inc [Online]. Available: https://www.gelest.com/product/DMS-T21/. [Accessed: 26-Jan-2022].

[18] Howell, L. L., Magleby, S. P., and Olsen, B. M., 2013, *Handbook of Compliant Mechanisms*, John Wiley & Sons, Inc, Chichester, West Sussex, United Kingdom Hoboken, New Jersey.